Nonlinear optimals in the asymptotic suction boundary layer: Transition thresholds and symmetry breaking

Draft version of: S.Cherubini, P. De Palma, J.C. Robinet, Non linear optimals in the asymptotic suction boundary layer, Physics of Fluids, American Institute of Physics, 2015, 27, pp.1.4916017. doi:10.1063/1.4916017

Non linear optimals in the asymptotic suction boundary layer: transition thresholds and symmetry breaking

S. Cherubini[1], P. De Palma[2], J.-Ch. Robinet[1]

[1] *DynFluid Laboratory, Arts et Metiers ParisTech, 151, Bd. de l'Hopital, 75013 Paris, France*

[2] *DMMM, CEMeC, Politecnico di Bari, Via Re David 200, 70125 Bari, Italy*

(Dated: December 2, 2014)

Abstract

The effect of a constant homogeneous suction on the non-linear transient growth of localized finite amplitude perturbations in a boundary-layer flow is investigated. Using a variational technique, *non-linear* optimal disturbances are computed for the asymptotic suction boundary layer (ASBL) flow, defined as those finite amplitude disturbances yielding the largest energy growth at a given target time T. It is found that a strong enough wall suction remarkably reduces the optimal energy gain in the non-linear case, and breaks the spanwise mirror symmetry which was a robust feature of the non-linear optimal perturbations found in the Blasius boundary-layer case. Symmetry-breaking appears when decreasing the Reynolds number from 10000 to 5000. Direct numerical simulations show that the different structure of the base flow leads to a different evolution of the symmetric or non symmetric initial perturbation, due to the transport and tilting of the vortices by the mean flow. By bisecting the initial energy of the non-linear optimal perturbations, minimal energy thresholds for subcritical transition to turbulence have been obtained. These energy thresholds are found to be 1 to 4 order of magnitude lower than the ones found in the literature for other transition scenarios. For low to moderate Reynolds numbers, these thresholds are found to scale as Re^{-2}, suggesting a new scaling law for transition in the ASBL.

PACS numbers:

Keywords:

I. INTRODUCTION

Drag reduction in external and internal flow is a fundamental topic in fluid mechanics since it is a key issue for improving the performance of engineering systems, increasing energy saving, and reducing environmental impact. Flow suction through the wall was among the first techniques applied to control the structure of the boundary layer in order to reduce drag. The idea, was born together with the concept of boundary layer itself [1], described for the first time in 1904 by Prandtl during the Third International Mathematics Congress at Heidelberg [2]. About thirty years later, such a technique was employed to delay transition over aircraft wings by reducing the boundary layer thickness and inducing a fuller velocity profile close to the wall [1]. The influence of suction on the stability of the boundary layer was studied by analytical methods considering uniform suction velocity at wall. In particular, a very simple exponential solution for the velocity was derived by Meredith and Griffith [1, 3] which would be valid at a sufficiently high distance from the leading edge of a flat plate. This solution of the Navier-Stokes equation is known as the asymptotic suction boundary layer (ASBL) [1] and is considered a suitable model to study boundary layers subject to active control by suction and to investigate the transition mechanism. Hocking (1975) [4] demonstrated that the critical Reynolds number is about two orders of magnitude higher than that of the Blasius boundary layer (BBL). In fact, the normal velocity term in the Orr-Sommerfeld and Squires equations stabilizes the Tollmien-Schlichting (TS) waves, producing an effective way of damping their asymptotic growth. This effect has been widely employed in different forms in the design of aircraft wing (see, for example, Joslin (1998) [5]).

More recently, the development of the optimal transient growth analysis has renewed the interest in the study of the ASBL. In fact, it is well known that for a sufficiently high level of free-stream turbulence (FST), a bypass route to transition may occur in the boundary layer which corresponds to the growth of linear optimal perturbations (LOP) [6, 7]. This mechanism is based on the development of streamwise-aligned structures composed by alternating low and high velocity streaks observed for the first time by Klebanoff [8]. The algebraic growth of the streaks due to the lift-up effect [9] leads eventually to secondary instability and break-up to turbulence [10–12]. From a numerical point of view, LOPs were computed for several shear flows [13–17]. In all of these works, optimal perturbations are defined as those initial flow states yielding the largest amplification of the disturbance energy

over a time/space interval and can be computed using a variational optimization approach [18, 19]. For the case of the boundary layer at low Reynolds number, such optimal structures consists of pairs of streamwise aligned counter-rotating vortices producing streamwise streaks by the lift-up effect, in perfect agreement with the above experimental findings. The same mechanisms have been studied in the ASBL. Fransson and Alfredsson (2003) [20] performed an experimental analysis about the development of forced TS waves and about the algebraic growth of disturbances induced by free-stream turbulence. They confirmed the damping of TS waves due to suction and were able to suppress transition in both cases. Using a local approach, Fransson and Corbett (2003) [21] computed LOPs for the ASBL and compared their results with experiments. They observed a significant transient growth, although smaller than in the case of the BBL. This indicates that the strong effect of the damping of the energy growth of TS waves obtained by suction is not achieved in the case of the algebraic growth. Bystrom et al. (2007) [22] computed LOPs for the semi-suction boundary layer in order to take into account the presence of a small region free of suction close to the leading edge of the flat plate. Using such a model, they could improve the agreement of the numerical results with experimental data, demonstrating that the optimal energy growth is indeed obtained in the upstream region without suction. Finally, Levin et al. (2005) [23] studied the energy thresholds for transition to turbulence in the ASBL, for $Re = 500,\ 800,\ 1200$, with perturbations having the form of oblique waves, streamwise vortices, or random noise; whereas, Levin et al. (2007) [24] analyzed the energy threshold for the same Reynolds numbers in the case of localized disturbances and investigated the formation and evolution of turbulent spots.

The ASBL has been also considered for testing and validating the recent dynamical system theory of turbulence, which analyzes the role of non-linearities in the transition process and for the sustainment of turbulence for shear flows. Such a theory relies on: 1) the observation of the existence of exact coherent states, which can be unstable fixed points, periodic orbits or chaotic solutions of the Navier-Stokes equations, having a few unstable directions (see Ref. [25–30]); 2) the idea that such states constitute the skeleton of transition and regeneration processes of turbulence and can be used to understand their nature. In particular, for analyzing the transition process, it is interesting to study those flow perturbations confined on the boundary between the laminar and the turbulent states, called the *edge of chaos* [31–34]. Those perturbations can be very dangerous, being the closest ones to the

laminar state capable of triggering transition. On the edge of chaos, one or more relative attractors can be found, called *edge states* [31], which can be fixed points [35], periodic orbits [36] or chaotic states [29]. Concerning the ASBL, Kreilos et al. (2013) [36] investigated the structure of the edge states, identifying a periodic orbit embedded in the laminar-turbulent boundary. Such a solution shows the same basic mechanisms of transient growth interactions between streamwise-aligned vortices and streaks which characterize many other shear flows. Furthermore, it captures also the bursting phenomenon typical of the BBL. Khapko et al. [37, 38] have investigated the dynamics restricted to the laminar-turbulent boundary, describing the complex spatio-temporal dynamics of different localized edge states for several streamwise wavelength. They found that all of these states have the same structure, consisting of a localised pair of low- and high-speed streaks flanked with streamwise vortices. Investigating the structure of the relative attractors embedded in the edge of chaos allows one to identify the typical shape and dynamics of the coherent structures consituting the skeleton of turbulence. However, for unraveling the main features of the most effective (in terms of both time and energy) path to transition, the minimal-energy states on the laminar-turbulent boundary should be analyzed [39, 40].

Very recently, the problem of finding the minimal energy perturbation on the edge of turbulence has been investigated by solving the non-linear optimal growth problem for finite-amplitude initial perturbations (see [41] for a review). Perturbations optimizing at a given (target) time the growth of a functional linked to transition (the kinetic energy or the dissipation, for instance), called non-linear optimal perturbations (NLOPs), have been discovered for a pipe flow [42, 43]; a boundary layer flow [44, 45]; and a Couette flow [34, 39, 46, 47]. By optimizing the energy at large target times and bisecting the initial energy to bring the perturbation close to the laminar-turbulent boundary, the perturbation of minimal energy capable of bringing the flow to the edge state and then to transition, called the *minimal seed* of turbulent transition, can be found [39]. When small target times are considered, a different procedure should be used for finding minimal-energy perturbations on the edge of chaos, directly targeting the neighbourhood of the edge state in a finite time [40].

In any case, the NLOPs are characterized by a very different structure with respect to the linear optimal ones and largely outgrow them in energy due to non-linear mechanisms [43, 45]. For the boundary-layer and the Couette flow, the NLOPs are characterized by a similar fundamental structure, composed of a localized array of vortices and low-momentum regions

of typical length scale, capable of maximizing the energy growth most rapidly. Cherubini et al. (2011) [45, 48] have discussed the contribution of non-linear effects to such a strong energy growth mechanism, showing that non-linearity is crucial to sustain the growth of these optimal perturbations. The knowledge of these non-linear mechanisms may allow one to design effective control strategies to delay transition by using wall suction or spanwise oscillations of the boundaries [49, 50]. The aim of the present paper is to extend the analysis of the NLOP to the case of the ASBL, following the approach that the authors have employed for the BBL, discussing similarities and differences between these two cases, and highlighting the role of the suction velocity.

The paper is organized as follows. In the second section we define the problem and describe the non-linear optimization method. In the third section, divided into three parts, a thorough discussion of the results of the non-linear optimization analysis is provided. In particular, in the first part, the focus is on the characterization of the NLOP with respect to the LOP, also using the comparison with the results already obtained for the BBL and Couette flows. The second part provides an analysis varying the Reynolds number, achieving supercritical values; whereas, the third part deals with the optimal route to turbulence, computed by the DNS. Finally, concluding remarks are provided.

II. PROBLEM FORMULATION

A. Governing equations and numerical method

The behaviour of an incompressible flow is governed by the Navier–Stokes (NS) equations:

$$\begin{aligned} &\frac{\partial \mathbf{u}}{\partial t} + (\mathbf{u}\cdot\nabla)\mathbf{u} = -\nabla p + \frac{1}{Re}\nabla^2\mathbf{u}, \\ &\nabla\cdot\mathbf{u} = 0, \end{aligned} \tag{1}$$

where $\mathbf{u} = (u, v, w)$ is the velocity vector and p indicates the pressure term. Dimensionless variables are defined with respect to the inflow boundary-layer displacement thickness δ^* and the freestream velocity, U^*_∞, so that the Reynolds number is $Re = U^*_\infty \delta^*/\nu^*$, where ν^* is the kinematic viscosity and the superscript * indicates dimensional quantities. A Cartesian coordinate system is considered, x, y and z being the streamwise, wall-normal and spanwise directions, respectively. The asymptotic suction boundary-layer flow is defined as the flow

over a flat plate with a uniform wall-normal suction velocity $V_S^* = \nu^*/\delta^*$ applied along the wall. Therefore, imposing no-slip conditions for the streamwise and spanwise components of the velocity at the wall, one obtains from equations (1) the following solution [3], given in nondimensional variables:

$$\mathbf{U} = ((1 - e^{-y}), -\frac{1}{Re}, 0)^T. \tag{2}$$

The numerical simulations are performed by integrating the NS equations with the following boundary conditions: at the bottom boundary, no-slip conditions for the x and z components of the velocity and homogeneous suction for the y component, $v = -V_S$; at the upper boundary, the z component of the velocity and of the vorticity are set to zero and homogeneous injection is imposed for the y component of the velocity; in the streamwise and spanwise directions, periodicity is imposed for the three velocity components and the pressure.

The analysis has been performed using five values of the Reynolds number (see table I), obtained changing the boundary-layer displacement thickness δ^* and keeping U_∞^* fixed. Thus, the suction velocity, in both dimensional and nondimensional forms, scales with the inverse of the Reynolds number, since $V_S^* = U_\infty^*/Re$. The NS equations are discretized by a finite-difference fractional-step method using a staggered grid [51]. A second-order-accurate centered space discretization is used. Performing a grid-convergence analysis, a mesh made up by $451 \times 100 \times 61$ points has been selected for the reference domain at $Re = 610$ with dimensions $L_x = 100$, $L_y = 20$ and $L_z = 10.5$. The spanwise dimension has been chosen very close to the one used in [23] for determining transition thresholds, whereas the streamwise length is much longer to avoid interaction of the flow structures with its own tail for long target times. Since the NLOP has been found to localize more and more with increasing Reynolds number, the domain length has been reduced accordingly, in order to reduce the computational cost. Table I summarizes the domain lengths and the corresponding grid points selected for different Reynolds numbers after validations with respect to larger domains. For all the values of the Reynolds number and of the target times considered here, the streamwise length of the domain has been chosen large enough to allow the optimal perturbation to remain localized also at target time. Whereas, concerning the spanwise length, it has been reduced with Re following the typical scaling of the streaks spacing, as explained in section III B.

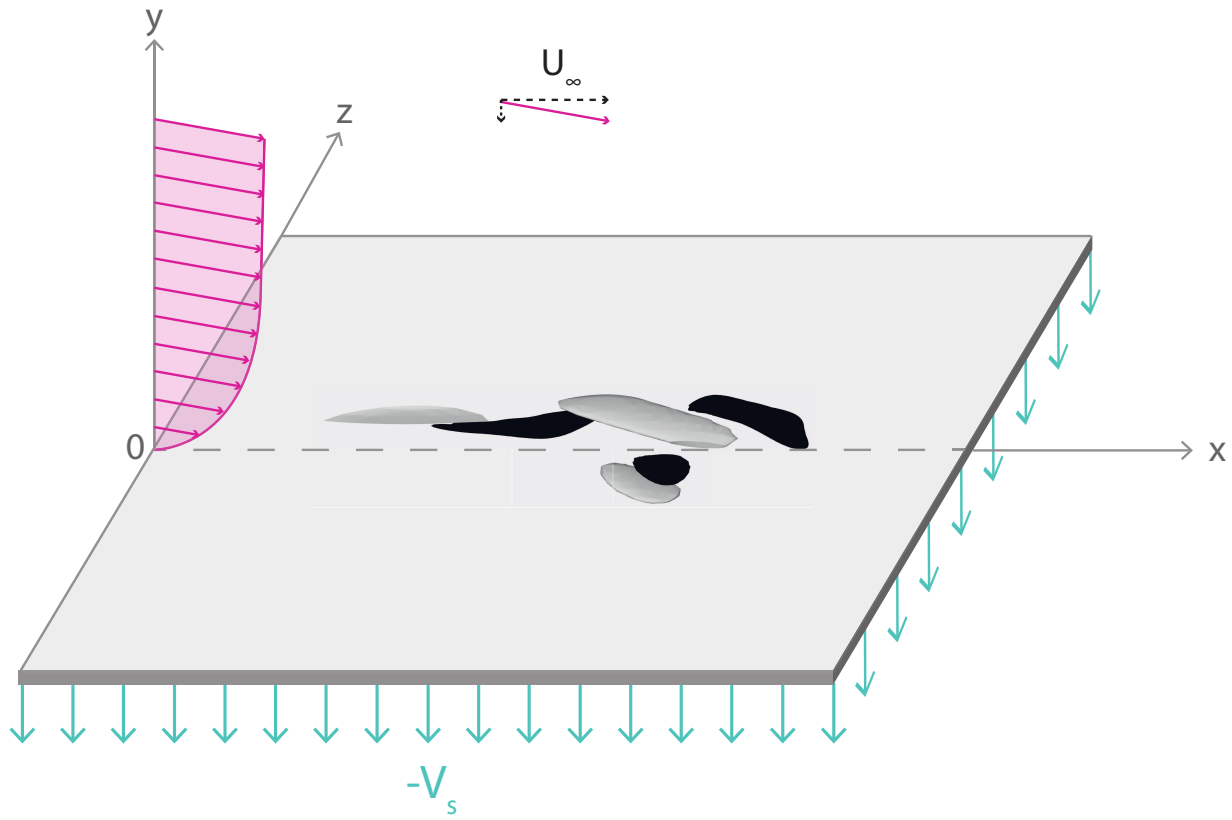

Figure 1: Sketch of the ASBL flow with a superposed localized disturbance.

Re	$L_x \times L_y \times L_z$	$N_x \times N_y \times N_z$	T
610	$100 \times 20 \times 10.5$	$451 \times 101 \times 61$	$50, 75, 100, 150, 200, 250$
1200	$50 \times 15 \times 7$	$451 \times 101 \times 61$	$50, 100, 150$
2500	$40 \times 15 \times 5$	$451 \times 101 \times 61$	$50, 100, 150$
5000	$40 \times 7.5 \times 4$	$451 \times 101 \times 91$	$50, 100, 150$
10000	$30 \times 7.5 \times 2$	$601 \times 101 \times 91$	$50, 100$

Table I: Domain lengths, grid points and target times chosen for the optimizations at different Reynolds numbers

B. Non linear optimization

The non-linear behavior of a perturbation $\mathbf{q} = (u', v', w', p')^T$ evolving in the laminar asymptotic suction boundary-layer flow is analyzed by solving the NS equations written in perturbative formulation with respect to the steady state solution, $\mathbf{Q} = (\mathbf{U}, P)^T$, with $\mathbf{U}$

given by equation (2). A zero perturbation boundary condition is imposed for the three velocity components at the $y-$constant boundaries, whereas periodicity of the perturbation is forced in the spanwise and streamwise directions.

The goal is to find the perturbation at $t = 0$ providing the largest disturbance growth at a given target time, T. At this purpose, a Lagrange multiplier technique is used [19, 42, 44, 52] to perform a constrained optimization of the perturbation energy. The disturbance energy density is defined as

$$E(t) = \frac{1}{2V} \int_V \left[u'^2(t) + v'^2(t) + w'^2(t) \right] dV = \frac{1}{2V} \left\langle \mathbf{u}'(t) \cdot \mathbf{u}'(t) \right\rangle , \tag{3}$$

where V is the volume of the computational domain. Given an initial energy $E(0) = E_0$, we aim at finding the shape and amplitude of an initial perturbation $\mathbf{q}_0$ which induces at target time T the largest energy gain $E(T)/E_0$; threfore, the objective function of the optimization procedure is $\Im = E(T)/E(0)$. The Lagrange multiplier technique consists in searching for extrema of an augmented functional, $\mathcal{L}$, with respect to every independent variable, the three-dimensional incompressible NS equations and the value of the initial energy being imposed as constraints. The augmented functional reads:

$$\begin{aligned} \mathcal{L} = \frac{E(T)}{E(0)} - \int_0^T \left\langle \mathbf{u}^\dagger \cdot \left\{ \frac{\partial \mathbf{u}'}{\partial t} - \mathbf{u}' \cdot \nabla \mathbf{U} + \mathbf{U} \cdot \nabla \mathbf{u}' + \mathbf{u} \cdot \nabla \mathbf{u}' - \nabla p' - \frac{\nabla^2 \mathbf{u}'}{Re} \right\} \right\rangle dt \\ - \int_0^T \left\langle p^\dagger \cdot \nabla \mathbf{u}' \right\rangle dt - \lambda \left(\frac{E_0}{E(0)} - 1 \right) . \end{aligned} \tag{4}$$

where $(\mathbf{u}^\dagger, p^\dagger, \lambda)$ are the Lagrange multipliers, e.g. the adjoint variables. Integrating by parts and setting to zero the first variation of $\mathcal{L}$ with respect to $(\mathbf{u}', p')$ leads to the adjoint equations plus the compatibility condition (which are provided in Ref. [45]). The adjoint equations are linked to the direct ones by the presence of the direct variables in the advection terms, so that the whole flow field needs to be stored at each time step, requiring a remarkable storage capacity. The gradient of the augmented functional with respect to the initial perturbation $\mathbf{q}_0$ is forced to vanish by means of a conjugate gradient algorithm as detailed in Ref. [45]. A coupled iterative approach similar to that used in [52] and [42] is used to solve the problem, relying on the forward and backward solution of the direct and adjoint NS equations, respectively, and on the update of the initial perturbation in the conjugate gradient direction at each iteration, until convergence is reached. A detailed description of the optimization technique and of its convergence properties is provided in Ref. [45] for the case of the BBL flow and in Ref. [47] for the Couette flow.

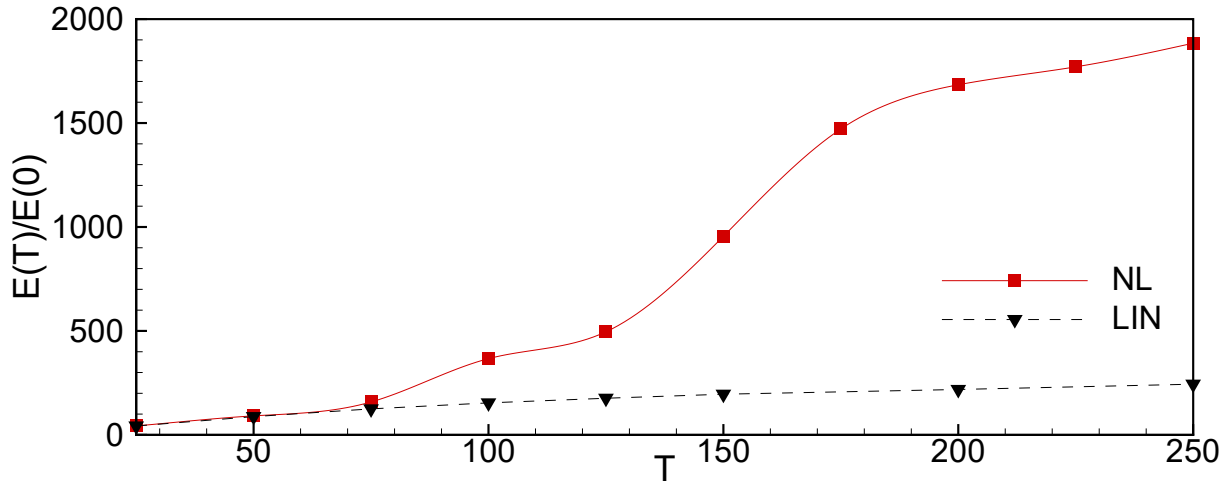

Figure 2: (Color online) Optimal energy gain versus target time T for $Re = 610$, $E_0 = 3.0 \times 10^{-7}$. The dashed line with triangles indicates the results of the linear optimization; the solid line with squares (red online) indicates the results of the non-linear optimization.

III. RESULTS

A. Non linear optimal perturbations at $Re = 610$

The laminar profile of the ASBL defined in equation (2) is linearly stable for $Re < 54382$ [4], which is about 100 times the critical Reynolds for a Blasius boundary layer [1]. For starting the analysis, we choose a subcritical Reynolds number, $Re = 610$. This rather low Reynolds number (compared to the critical one for the ASBL) has been chosen for comparison purpose with the BBL case of ref. [44]. Figure 2 shows the value of the optimal energy gain versus the target time for an initial energy $E_0 = 3.0 \times 10^{-7}$. The dashed line refers to the results of a linear optimization, whereas the solid line represents the non-linear optimization. As also observed for the BBL flow [44], the non-linear optimal energy gain is remarkably larger than the corresponding linear one for $T > 50$. The influence of the parameter E_0 on the value of the optimal energy is shown in Figure 3, for three values of the target time. It appears that a *non-linearity threshold* value of the initial energy exists from which strong differences are observed in the non-linear optimal energy with respect to the linear one (compare the solid lines with the dashed ones). Such a threshold decreases when the target time increases, as one can observe by comparing the solid lines in Figure

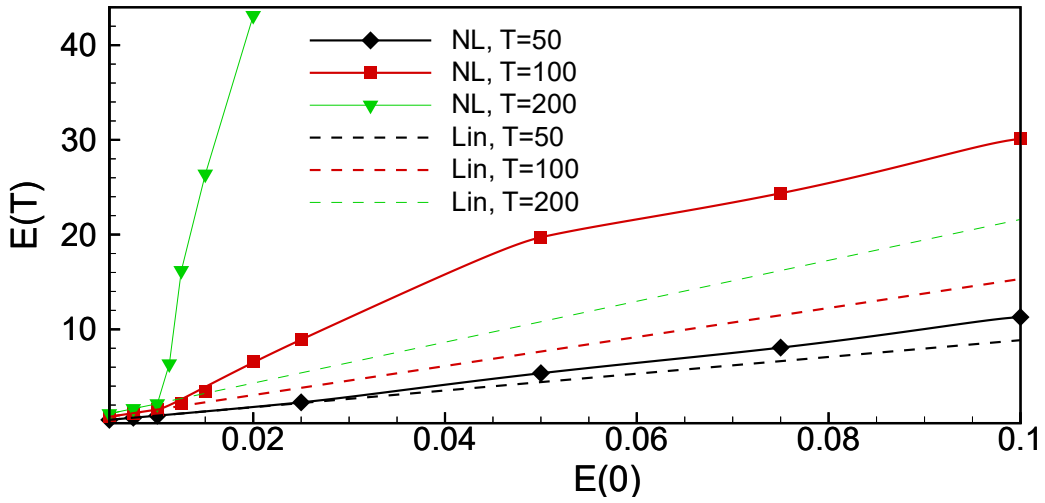

Figure 3: (Color online) Optimal energy for $Re = 610$ at target time $T = 50$ (black), $T = 100$ (red), and $T = 200$ (green) versus the initial energy $E(0)$, using the non-linear optimization (solid lines with symbols) and the linear optimization (dashed lines).

3, converging towards a value, $E_0 = 1.2 \times 10^{-7}$, which might be close to the energy of the minimal seed for this Reynolds number (i.e., the perturbation of minimal energy on the laminar-turbulent boundary). Table II provides a comparison between the energy gains obtained for the BBL and the ASBL at $T = 75$ (the behavior is similar for different target times) for three optimizations: a linear optimization and two non-linear optimizations with $E_0 = 1.2 \times 10^{-7}$ and $E_0 = 3.0 \times 10^{-7}$, respectively. The results indicate that a significant reduction of the optimal energy growth is obtained in the linear case; however, wall suction is much more effective in damping the growth of non-linear optimal perturbations.

Crossing the non-linearity threshold also yields large modifications in the shape of the optimal perturbations. This can be observed in Figure 4, which provides the optimal initial perturbations obtained for the ASBL at $Re = 610$ and $T = 75$, for two values of the initial energy, E_0. For the lowest one, $E_0 = 1.2 \times 10^{-7}$ (top frame), the perturbation is similar to that obtained by the linear optimization in a BBL flow [53], being characterized by alternated vortices elongated in the streamwise direction (black and white surfaces), localized in two different positions along the flat plate. Due to weak non-linear effects, which are non-negligible for such values of the initial energy, some spanwise modulations are present on the streamwise perturbation (green surfaces). Concerning the amplitudes, the largest

Test case	Linear	$E_0 = 1.2 \times 10^{-7}$	$E_0 = 3.0 \times 10^{-7}$
BBL	275.10	801.98	1104.1
ASBL	125.16	125.15	158.37

Table II: Comparison between energy gains at $T = 75$ for the BBL and the ASBL.

perturbation velocity component is the spanwise one ($|w_{max}| = 0.0027$), followed by the wall-normal ($|v_{max}| = 0.0025$) and the streamwise one ($|u_{max}| = 0.0003$). One can notice that the streamwise perturbation is one order of magnitude lower than the others, meaning that for this value of the initial energy the mechanism of growth is still very close to the linear optimal one, based on the *lift-up* of the streamwise base flow velocity by the vortices formed by the wall-normal and spanwise perturbation. However, as one can observe in figure 4, the shape of the optimal perturbation changes remarkably between $E_0 = 1.2 \times 10^{-7}$ and $E_0 = 3.0 \times 10^{-7}$. The most striking difference is the strong localization of the disturbance in both the streamwise and spanwise direction. In fact, for initial energies larger than the non-linearity threshold, a strong localization of the initial perturbation leads to larger amplitudes (for the same initial energy), triggering non-linear effects that induce a remarkable increase of the energy gain at target time. In fact, for an increase of the initial energy of a factor 2.5, we observe at $t = 0$ an increase of the velocity magnitudes of a factor equal to about 12 for v and w, whereas a factor 80 is obtained for u. These values of the perturbation velocity components, together with the particular shape of the disturbance, are able to trigger non-linear effects which allow a much larger energy growth than in the linear case. This strong localization appears to be a typical feature of NLOPs in shear flows, since it has been also observed for the pipe [42, 43], the BBL [45], and the Couette flows [39, 46, 47]. Furthermore, not only the extension, but also the structure of the perturbation changes remarkably. For $E_0 = 3.0 \times 10^{-7}$, the optimal perturbation is composed by three streamwise-alternated vortices showing a finite inclination with respect to the streamwise direction (black and white surfaces), whereas in the quasi-linear case at $E_0 = 1.2 \times 10^{-7}$ the vortices are streamwise-aligned. On both flanks of such inclined vortices, localized patches of finite-amplitude streamwise disturbance are observed (green surfaces). Concerning the relative magnitude of the velocity perturbations, the largest perturbation velocity component is the spanwise one ($|w_{max}| = 0.033$), followed by the streamwise ($|u_{max}| = 0.03$) and the wall-

normal one ($|v_{max}| = 0.024$). These values are similar to those found for the Couette flow [47], whereas, for the BBL flow at the same Re, the largest component is the streamwise one, whose value is about half of the maximum value found here for the ASBL, for an initial energy just above the non-linearity threshold, see [45]. It is worth noticing that, for all of these flows, in the linear case the streamwise velocity component at initial time is from one to two orders of magnitude lower than the spanwise and the streamwise ones, whereas in the non-linear case all of the components are of the same order, clearly indicating that different mechanisms are responsible for the growth of the perturbation energy. It is also noteworthy that, for all of the values of E_0, the NLOPs are characterized by vortical structures inclined in the opposite direction with respect to that of the base flow, as one can observe in figure 4. In fact, it is known that perturbations inclined in the opposite direction with respect to the base flow allow a large growth of the energy at small times due to the tilting of the initial spanwise vorticity into the direction of the shear. Such a mechanism is called Orr mechanism [54] and it is typical of most of the optimal perturbations found for shear flows (see [53**? ?**], for instance), in a linear and non-linear framework. In our case, since the NLOPs perturbations are supposed to grow optimally, they should exploit all of the energy production mechanisms in order to trigger non linear effects as fast as possible.
The structure of the NLOP found here shows some similarities with that found for the Couette flow (compare with Figure 5 of Ref. [47]) and with that obtained for the BBL flow (see Figure 4, bottom). For all of these shear flows, the NLOP is characterized by streamwise-inclined vortical structures and finite-amplitude patches of streamwise disturbance. However, while for the Couette and the ASBL flow (at least at low Reynolds number) the optimal disturbance does not show any particular symmetry, for the BBL it is mirror-symmetric with respect to a $z = const$ plane. This can be clearly observed in Figure 4 (bottom frame), showing that the NLOP for the Blasius flow at $E_0 = 1.2 \times 10^{-7}$ is composed by a basic structure similar to that of the ASBL, having a mirror-symmetric shape with respect to a $z-$aligned plane.

The flow structures can be better analyzed by taking $x-$constant slices of the NLOP, as provided in the left frame of figure 5. One can observe that the inclined alternated vortices are strictly localized in a narrow zone in the spanwise direction ($2 < z < 5$), surrounded by patches of negative (light gray) and positive (dark gray) streamwise perturbation which are alternated in the spanwise and wall-normal direction. The differences with respect to

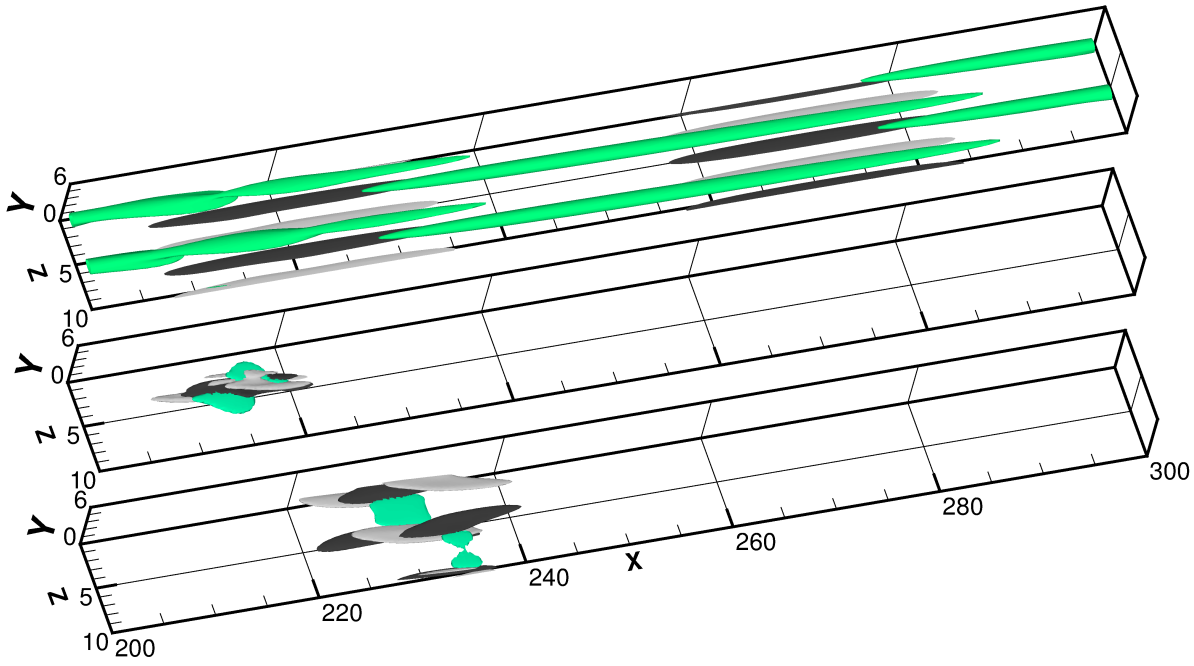

Figure 4: (Color online) Initial perturbations obtained by the non-linear optimization for the asymptotic suction boundary-layer at $Re = 610$ and target time $T = 75$: iso-surfaces of the optimal perturbations (grey, green online, for the negative streamwise component; dark and light gray for negative and positive streamwise vorticity, respectively) with initial energy $E_0 = 1.2 \times 10^{-7}$ (top frame, surfaces for $u' = -0.00017$, $\omega_x' = \pm 0.01$) and $E_0 = 3.0 \times 10^{-7}$ (middle frame, $u' = -0.015$, $\omega_x' = \pm 0.1$). Initial perturbations obtained by the non-linear optimization for the Blasius boundary layer flow at $Re = 610$, target time $T = 75$, with initial energy $E_0 = 1.2 \times 10^{-7}$ (bottom frame, $u' = -0.01$, $\omega_x' = \pm 0.06$). Axes are not in the same scale.

the BBL case can be analyzed by comparing the left frame (ASBL) with the right frame (BBL) of figure 5. Concerning the latter, the vortices are localized in two distinct regions in the spanwise direction, connected by alternated patches of streamwise disturbance showing a mirror-symmetry in the spanwise direction. This discrepancy is reflected also at target time, as one can notice comparing Figures 6 (a) for the ASBL, with (b), for the BBL. For the ASBL, one can observe in figure 6 (a)-(b) the presence of bent streaks along the streamwise vortices, showing strong oscillations in the streamwise and spanwise directions. Whereas, in figures 6 (c)-(d) one can notice that, for the BBL flow, the perturbations remain spanwise-symmetric, and the vortices as well as the streaks along them are strongly lifted in the wall-normal direction, showing the typical signature of an incipient hairpin vortex.

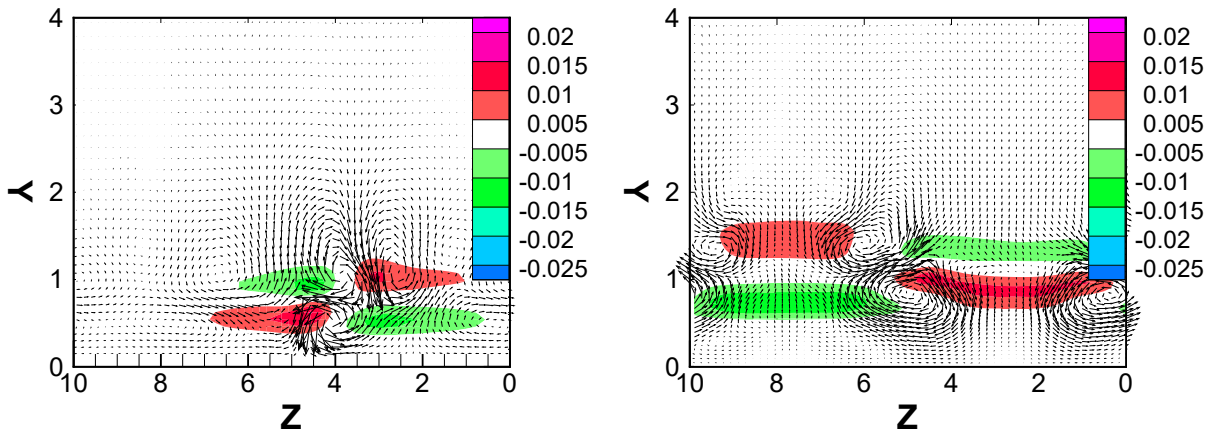

(a) (b)

Figure 5: (Color online) Contours and vectors of the velocity components of the NLOP at initial time obtained with $Re = 610$, $T = 75$ for the asymptotic suction boundary layer with $E_0 = 3.0 \times 10^{-7}$, on the plane $x = 211$ (a); for the Blasius boundary layer with $E_0 = 1.2 \times 10^{-7}$, on the plane $x = 232$ (b). Shaded contours indicate the streamwise disturbance velocity (dark, red online, for positive values; light, green online, for negative ones); vectors represent the wall-normal and the spanwise disturbance velocity components.

As proposed in Ref. [42], the disturbance of minimum amplitude capable of triggering turbulence is defined as the minimal seed for a given Reynolds number. Bisecting the value of the initial energy at $T = 200$, and checking whether the obtained NLOP is able to induce transition, we have found the energy level of the minimal seed to be about 1.277×10^{-7} for $Re = 610$. The corresponding maximum amplitudes of the velocity components are $|u|_{max} = 0.029, |v|_{max} = 0.031, |w|_{max} = 0.031$, very close to the values found at lower target time (even if the wall-normal component is now slightly larger than the streamwise one). The minimal seed is sandwiched between the NLOPs shown in figure 7 (a) and (b), for $E_0 = 1.2 \times 10^{-7}$ and $E_0 = 1.35 \times 10^{-7}$, both showing the basic structure provided in figure 4 (middle frame). It is worth noticing that the NLOP keeps the same structure of the minimal seed also for values of the initial energy slightly lower than the minimal seed energy. For larger values of the initial energy, local maxima can be found, as in the case of the Couette flow [47]. Furthermore, for energies larger than the minimal seed one, convergence on the optimum is not assured (see [39]), since transition might be observed at target time.

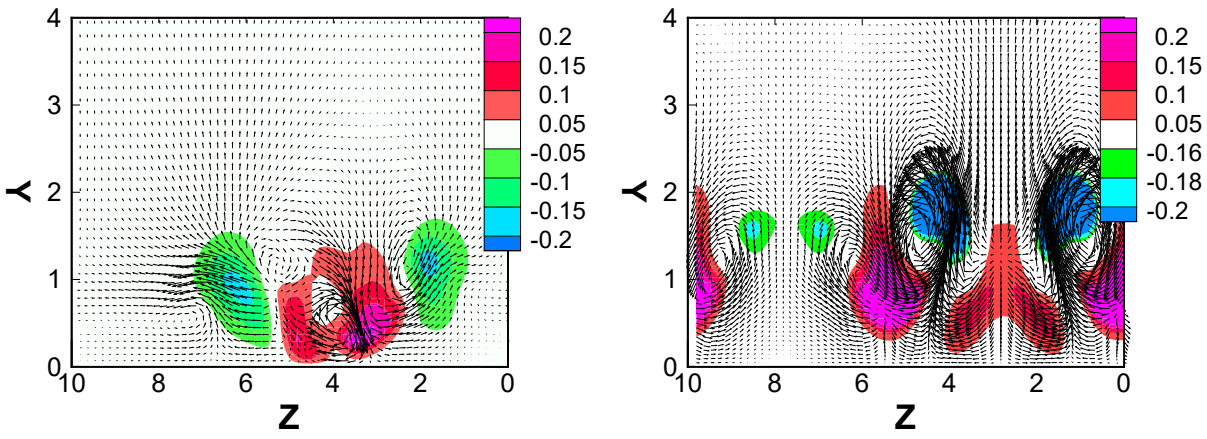

(a) (b)

Figure 6: (Color online) Contours and vectors of the velocity components of the NLOP at target time obtained with $Re = 610$, $T = 75$ for the asymptotic suction boundary layer with $E_0 = 3.0 \times 10^{-7}$ on the plane $x = 249$ (a); for the Blasius boundary layer with $E_0 = 1.2 \times 10^{-7}$ on the plane $x = 267$ (b). Shaded contours indicate the streamwise disturbance velocity (dark, red online, for positive values; light, green online, for negative ones); vectors represent the wall-normal and the spanwise disturbance velocity components.

However, since for $T = 200$ transition is still not observed for initial energies slightly higher than that of the minimal seed, we have been able to perform two optimizations with two different initial conditions, in order to check the existence of such local maxima. Thus, we have chosen $E_0 = 2.7 \times 10^{-7}$ (almost double than the energy of the minimal seed), with two different initializations, namely, i) the minimal seed structure, and ii) a symmetric initial disturbance obtained by mirroring the minimal seed structure with respect to the streamwise axis. The energy gain for the first optimization is $E(T)/E_0 = 1641$, and the optimal shape is shown in figure 7 (c); whereas, for a mirror-symmetric initial guess, the suboptimal structure shown in figure 7 (d) has been found, with energy gain $E(T)/E_0 = 254$ (even if the optimization eventually converges to the non symmetric solution if the convergence process is continued to lower values of the residual). The comparison between the optimal in figure 7 (c) and the suboptimal in figure 7 (d) proves that replication and spatial spreading of the basic structures is observed for large initial energies, as in the Couette flow, but this does not lead to a symmetrisation of the optimal (at least for $Re = 610$).

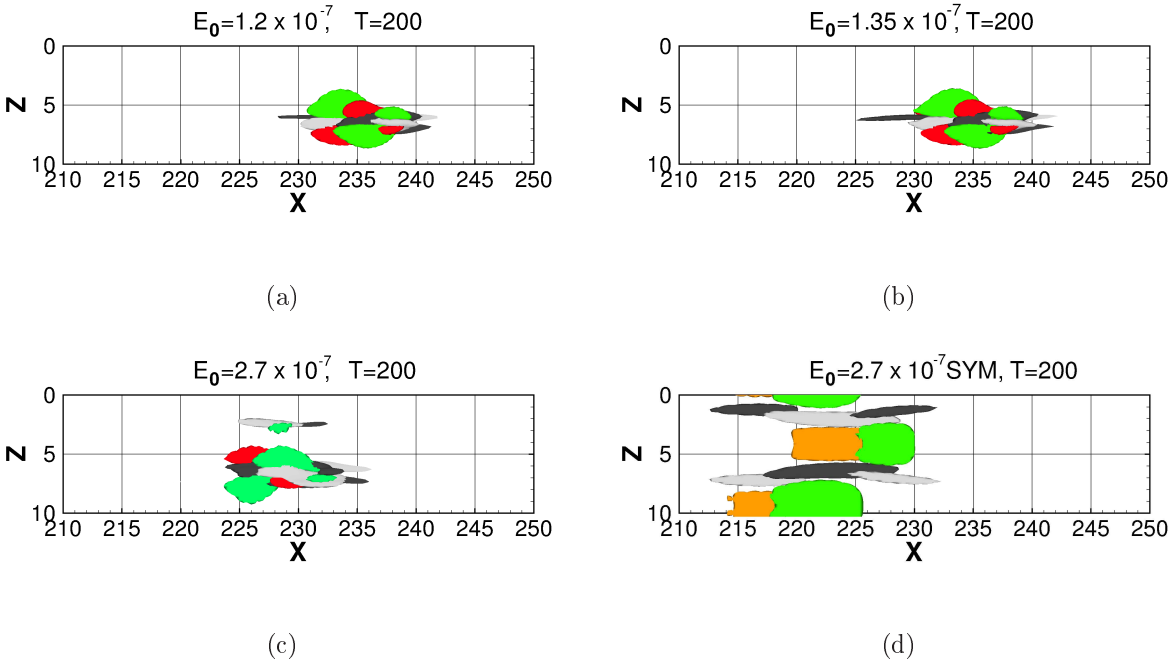

(a) (b)

(c) (d)

Figure 7: (Color online) Isosurfaces of the initial perturbations obtained by the non-linear optimization for the ASBL at $Re = 610$ and target time $T = 200$, with initial energies $E_0 = 1.2 \times 10^{-7}$ (a), $E_0 = 1.35 \times 10^{-7}$ (b), $E_0 = 2.7 \times 10^{-7}$ (c) and a suboptimal for $E_0 = 2.7 \times 10^{-7}$ initialized with a mirror-symmetric initial perturbation (d). Green and red, for the negative and positive streamwise velocity component; dark and light, for negative and positive streamwise vorticity, respectively, with values $u' = -0.005$, $\omega_x' = \pm 0.05$ (a-b), $u' = -0.01$, $\omega_x' = \pm 0.08$ (c), $u' = -0.005$, $\omega_x' = \pm 0.05$ (d).

The results discussed above show that NLOPs obtained for different shear flows share a similar structure, characterized by inclined vortices along a patch of finite streamwise velocity perturbation (although with a different symmetry). The persistence of this basic structure at different values of the initial energy, target times and for different kind of flows indicates that such a structure, which maximizes the disturbance energy over a finite time, has an intrinsic fundamental importance for shear flows. However, a crucial difference has been found between the basic structure of NLOP for the ASBL flow (similar to that of the Couette flow) and that for the BBL flows, namely, the spanwise symmetry of the perturbation. This important difference has motivated the analysis of the structure of the NLOP for several Reynolds numbers provided in the next subsection.

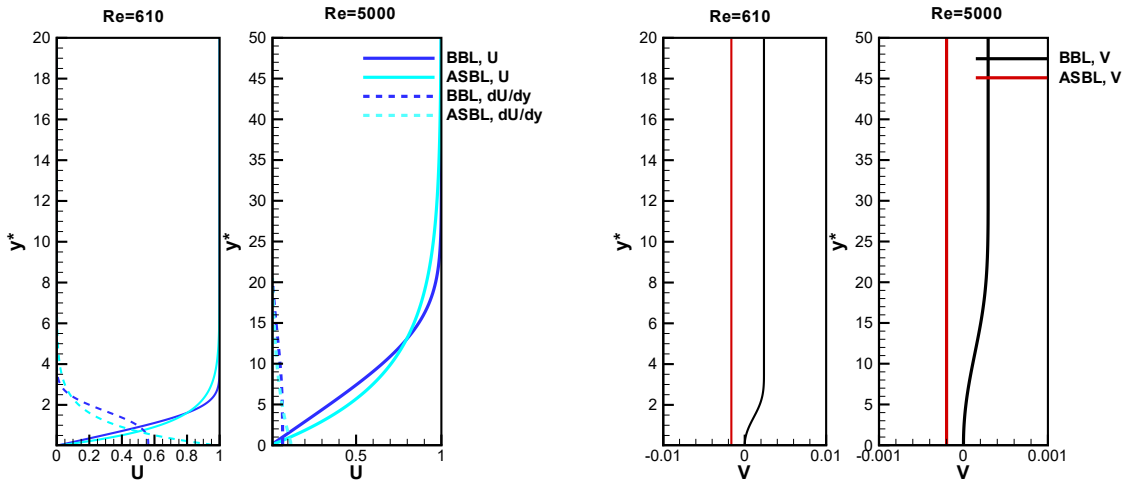

Figure 8: Streamwise (left) and wall-normal (right) velocity profilesof the base flow velocity for the BBL and the ASBL at $R = 610$ (thin solid lines) and $Re = 5000$ (thick solid lines), versus the wall-normal variable y^*. For visualization purposes, the scale is not the same at different values of Re. The dashed lines in subfigure (a) show the wall-normal derivative of the streamwise component of the base flow, dU^*/dy^*, in both flows.

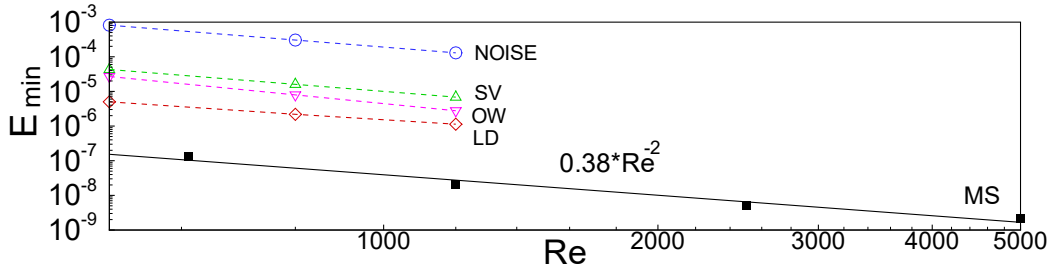

Figure 9: Minimal energy for turbulent transition for the asymptotic suction boundary layer at different Reynolds numbers (solid line). The dashed lines show the minimal energy for different transition scenarios, namely noise (NOISE), streamwise vortices (SV), oblique waves (OW), and localized disturbances (LD), extrapolated from data in [24].

B. Reynolds number analysis

To generalize our results, we have extended the analysis to larger Reynolds numbers. Figure 8 shows the velocity profiles for the ASBL and the BBL (extracted at the inlet) at two different Reynolds numbers, namely, $Re = 610$ and $Re = 5000$, versus the wall-normal

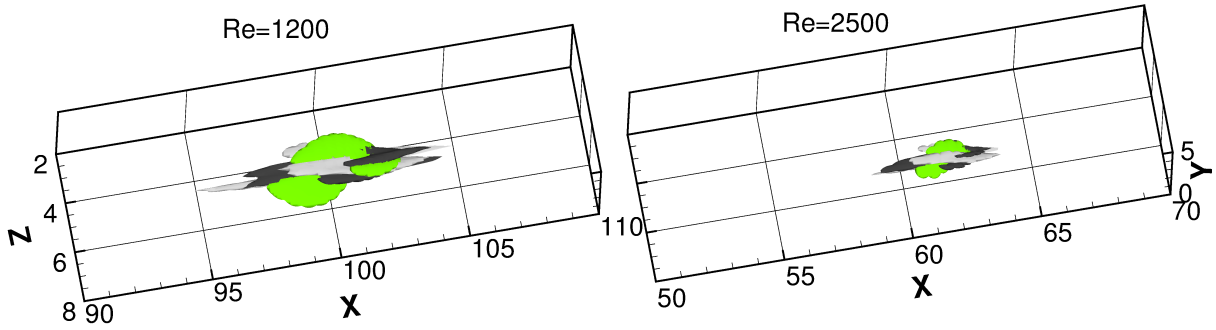

Figure 10: (Color online) Minimal seeds for the asymptotic suction boundary layer for $Re = 1200$ (left, with $E_0 = 2.08 \times 10^{-8}$) and $Re = 2500$ (right, with $E_0 = 4.16 \times 10^{-9}$) with target time $T = 150$: iso-surfaces of the negative streamwise component, $u' = -0.0025$ (green) and of the negative and positive streamwise vorticity, $\omega'_x = -0.045$ (black and white, respectively)

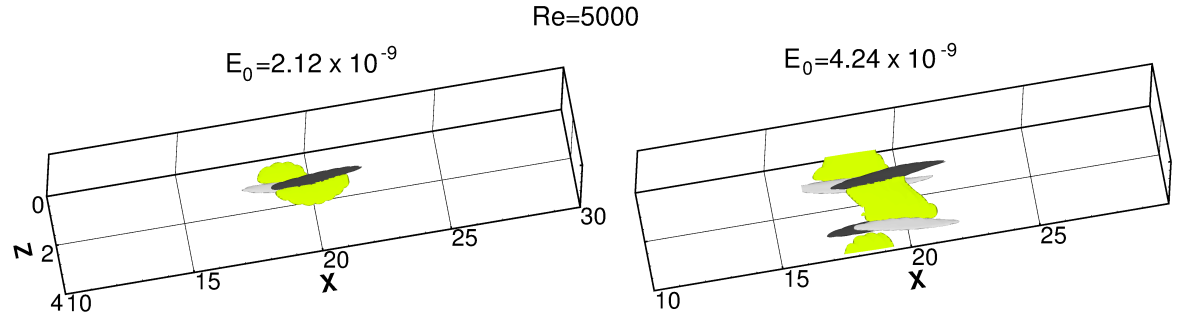

Figure 11: (Color online) Non linear optimal perturbations for the asymptotic suction boundary layer at $Re = 5000$ for $E_0 = 2.12 \times 10^{-9}$ (left) and $E_0 = 4.24 \times 10^{-9}$ (right) with target time $T = 100$: iso-surfaces of the negative streamwise component, $u' = -0.001$ (green) and of the negative and positive streamwise vorticity, $\omega'_x = \pm 0.045$ (black and white, respectively)

coordinate y^* (for visualization purposes, the scale is not the same at different values of Re, and $\delta^* = 1$ has been chosen for $Re = 610$). The figure shows that, for both flows, the streamwise profile is the same at $Re = 610$ and $Re = 5000$ except for the different scaling with respect to the wall-normal coordinate y^*. One can also notice the different shape of the ASBL and BBL profiles, the first one having larger velocities close to the wall, resulting in a 'fuller' shape close to the wall. Concering the wall-normal velocity, for both flows, an increase of one order of magnitude in the Reynolds number induces a decrease of one order

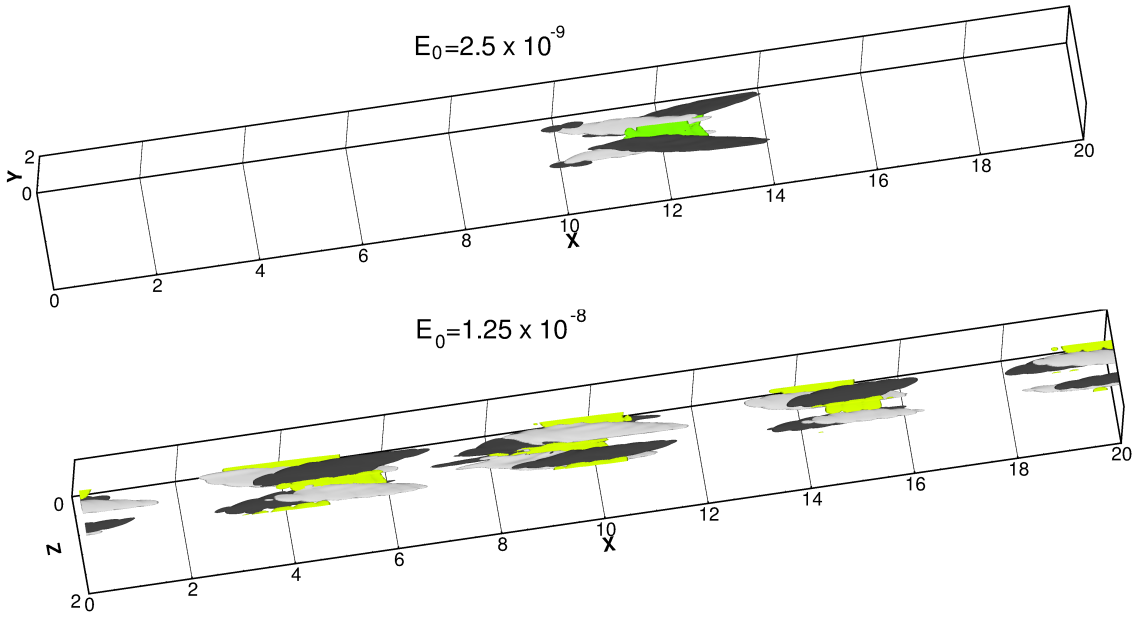

Figure 12: (Color online) Non linear optimal perturbations for the asymptotic suction boundary layer at $Re = 10000$ with $E_0 = 2.5 \times 10^{-9}$ (top), and with $E_0 = 1.25 \times 10^{-8}$ (bottom) with target time $T = 50$: iso-surfaces of the negative streamwise component, $u' = -0.002$ (green) and of the negative and positive streamwise vorticity, $\omega'_x = \pm 0.045$ (black and white, respectively)

of magnitude in the amplitude of the wall-normal velocity profile V (figure 8 (b)).
The non-linear optimal disturbances of the ASBL flow have been computed for $Re = 1200, 2500, 5000, 10000$. For each value of the Reynolds number but the latter the value of the initial energy has been bisected in order to approximate the minimal seed with a two-digit accuracy. The solid line in Figure 9 shows the energy of the minimal seed, E_{min}, versus the Reynolds number, for $Re = 610, 1200, 2500, 5000$. Whereas, the dashed lines in the figure reproduce the results of Ref. [23, 24], for four different initial perturbation structures: i) random three-dimensional noise (NOISE); ii) streamwise vortices (SV), obtained by a local spatial optimization; iii) spatially extended oblique waves (OW), obtained by a local spatial optimization; iv) localized disturbances (LD) consisting of two alternated counter-rotating pairs of streamwise vortices. One can notice that the transition threshold provided by the minimal seed energy is almost two orders of magnitude lower than the energy thresholds found for spatially extended disturbances such as the streamwise vortices and the oblique waves. Moreover, E_{min} is one order of magnitude lower than the minimal energy found for

$Re =$	610	1200	2500	5000	10000
$l_x =$	18.2	8.6	4.1	2.9	1.7
$l_z =$	8.6	4.4	2.7	1.94	1.3

Table III: Streamwise and spanwise dimensions, l_x, l_z of the minimal seed for several values of the Reynolds number, measured as the largest spanwise and streamwise lengths of the flow regions where $|u'| > 0.001$

the localized perturbations selected in Ref. [24]. We can also observe in figure 9 that E_{min} varies with Re following a power law Re^{-2}, whereas Levin et al. [23] found a -2.1 exponent for the SV and NOISE perturbations and a -2.8 exponent for the OW one. It is worth noticing that in Ref. [34], a power law $Re^{-2.7}$ has been found for the minimal seed for the Couette flow in a small domain (whereas the OW scenario was characterized by a -2 exponent for the same configuration). Concerning the velocity amplitudes, for $Re = 1200$ the minimal seed is characterized by $|u|_{max} = 0.014, |v|_{max} = 0.015, |w|_{max} = 0.017$; the minimal LD triggering transition in Ref. [24] was characterized by $|v|_{max} = 0.0124$, very close to the minimal amplitudes found here, but with $|u|_{max} = 0.0$. Thus, the large difference in the transition thresholds can be linked to the complete absence of the streamwise velocity in the perturbation of Ref. [24]: this appears to be a crucial feature for inducing a rapid transition to turbulence using low-energy perturbations. Two other crucial elements which might explain the difference between the energy thresholds for the LD and the minimal seed are: i) the larger spatial extension of the LDs, which makes them more energetic than the minimal seed for similar associated amplitudes; ii) the fact that the vortices are perfectly aligned with the streamwise axis, and sinusoidal in z, whereas the perturbations inducing the largest growth by non-linear mechanisms are characterized by a finite inclination with respect to the streamwise axis and do not show any spanwise symmetry. Thus, it appears that a non-linear optimization is necessary to evaluate the order of magnitude of the minimal thresholds for transition to turbulence and to determine accurately the shape and typical length scales of the minimal perturbation capable of inducing transition to turbulence.

As shown in Figure 10, the shapes of the minimal seed for $Re = 1200$ and $Re = 2500$ are very similar to the ones described in the previous section for $Re = 610$. They are composed by streamwise alternated positive and negative vortices with a finite inclination with respect

to the streamwise and wall-normal axis. It is worth noticing that, even if the basic structure is the same, the minimal seed is much more localized for higher values of the Reynolds number, as shown in table III. In particular, the streamwise and spanwise lengths appear to be almost halved for an increase of Re of a factor two.

For a fluid with a given kinematic viscosity, the dependence on Re of the typical length scales of the wall-structures, such as the streaks, is more complex in the case of the ASBL than in the case of the BBL. For the ASBL the Reynolds number can be varied either by changing the freestream velocity U^*_∞ (keeping the suction velocity fixed), or by changing the suction velocity, thus modifying the displacement thickness δ^* (keeping U^*_∞ fixed). Yoshioka et al. [55] have experimentally measured the typical length scales of the wall structures induced by free stream-turbulence in the ASBL, concluding that: i) if V^*_S and δ^* are kept constant, the spanwise spacing of the streaks varies with $(U^*_\infty)^{-1}$; ii) if U^*_∞ is kept constant and δ^* is changed, the dimensional spacing of the streaks remains constant. In the present work, we change the Reynolds number by keeping U^*_∞ constant, modifying the suction velocity V^*_S; therefore, we are increasing the reference length, δ^*, when the Reynolds number increases. Thus, a decrease of a factor 2 of the minimal seed size corresponding to a twofold increase of the reference length δ^* is consistent with the results in Ref. [55], since the dimensional typical length scales of the streaks will not change with Re when U^*_∞ is kept constant. We can thus conclude that, at least for Reynolds numbers in the range $[610, 10000]$, the typical length scales of the NLOPs change accordingly to the streak spacing measured in Ref. [55]. This explains why we have chosen to use smaller domain lengths for larger Re.

Another important feature of the minimal seed shown in figure 10 for $Re = 1200$ and 2500 is that, as for $Re = 610$, it does not present any symmetry in the spanwise direction. However, when the Reynolds number is increased to $Re = 5000$, two types of non-linear optimal solutions have been found. Figure 11 shows the results of the non-linear optimization for two initial energies, $E_0 = 2 \times 10^{-9}$ and $E_0 = 4 \times 10^{-9}$, for $T = 100$. One can observe that the latter is almost symmetric, roughly corresponding to a mirroring of the former with respect to the streamwise axis. The minimal seed for this Reynolds number is sandwhiched between these two solutions with different symmetries. Further bisections of the initial energy value, performed with a non-symmetric initial guess in order to not impose any symmetry, indicate that the minimal seed is not mirror-symmetric. However, the presence of a mirror-symmetric non-linear optimal perturbation is an indication of the change in the optimal dynamics that

is observed at larger Reynolds numbers. In fact, for $Re = 10000$, only mirror-symmetric optimal disturbances have been found. Figure 12 shows two of them for two energy levels and a short target time $T = 50$. This result has been verified by performing optimizations at a larger supercritical Reynolds number, $Re = 65000$, for which a symmetric minimal seed has been found as well, preserving the same structure. This indicates that a value of the Reynolds number exists between 5000 and 10000 for which the NLOP changes from a nonsymmetric shape to a symmetric one. Therefore, for sufficiently high Reynolds numbers, the structure of the minimal seed becomes similar to the one of the BBL. This behavior can be explained considering that we are changing the Reynolds number $Re = U^*_\infty/V^*_S$ by modifying the suction velocity V^*_S (keeping U^*_∞ fixed to a given value). Therefore, increasing the Reynolds number, while the streamwise velocity profile remains unchanged (with respect to the nondimensional wall-normal coordinate), the magnitude of V^*_S decreases. Comparing the streamwise and wall-normal velocity profiles at $Re = 610$ and $Re = 5000$ shown in figure 8, one can notice that for the latter value the difference between V_{ASBL} and V_{BBL} is reduced by one order of magnitude. Thus, we conjecture that the symmetry change of the NLOP at some "critical" Reynolds number is linked to such a reduction of the wall-normal velocity component. This conjecture may appear in contrast with the results in [20, 21], where a linear local transient growth analysis, performed for a hypothetical flow with no suction but an identical U-velocity profile to the ASBL, was found to bring only small differences on the transient energy gain as well as on the shape of the linear optimal with respect to the case in which the suction was considered as well. In this work, the authors concluded that the differences values of the optimal energy gain found for the ASBL and the BBL can be attributed to the change in shape of the mean streamwise velocity profile, not to the presence of the V base flow velocity. However, in the present work we are in a global, non-linear framework, in which the optimal can be localized and not sinusoidal in the spanwise and streamwise direction. Thus, the base flow wall-normal velocity V might have a considerable role in selecting the symmetry of the optimal, despite the basic structure of the optimal solution and the resulting linear amplification would be mostly driven by the streamwise velocity profile U.

In the next section we will compare the route to turbulence at low Reynolds number for the ASBL and the BBL, in order to understand how these differences in the base flow profiles can induce different symmetries on the non-linear optimal solutions. We will also link these

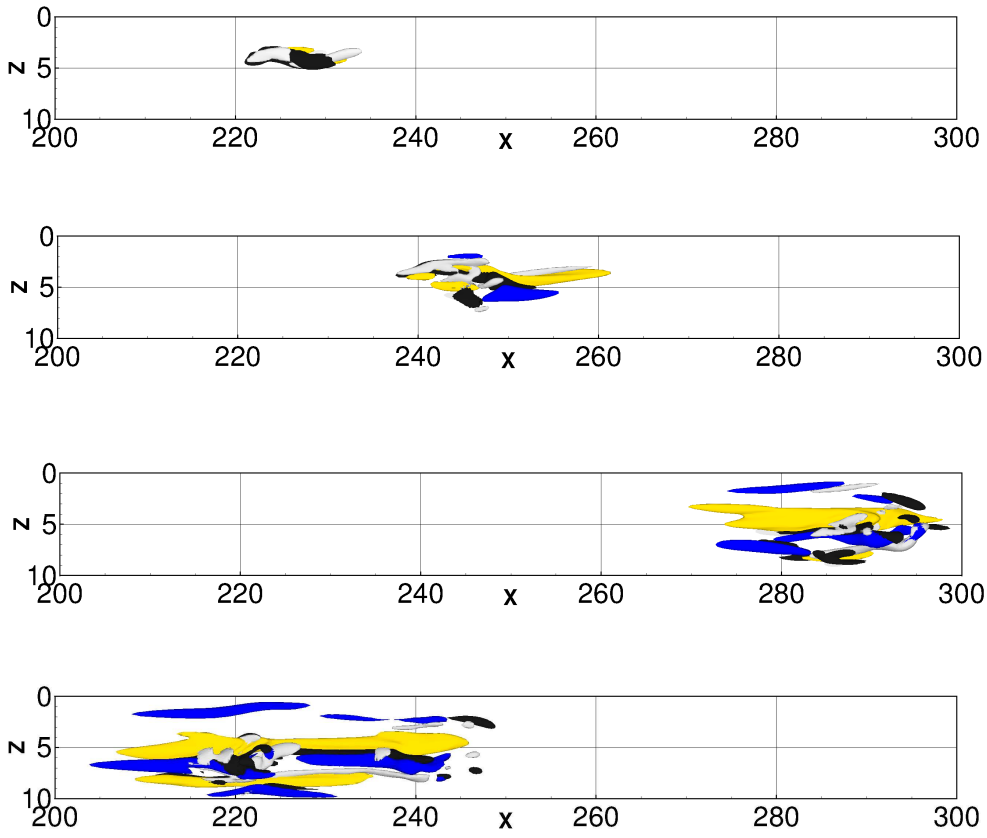

Figure 13: (Color online) Snapshots of the evolution in time of the selected NLOP for the ASBL: iso-surfaces of the streamwise velocity and vorticity perturbations (yellow and blue, for $u' = \pm 0.15$, respectively; black and white, $\omega'_x = \pm 0.2$, respectively) at $t = 40, 80, 140, 200$ (from top to bottom).

results to the change of symmetry observed at high Reynolds numbers in the ASBL.

C. The route of the non-linear optimal perturbations to turbulence

In this section, we analyze by DNSs the evolution towards turbulence of the NLOP obtained for the ASBL with $Re = 610$ and $T = 75$, providing a comparison with the NLOP of the BBL for the same conditions [45]. In order to achieve transition, the two perturbations have different energy, namely, $E_0 = 3.0 \times 10^{-7}$ for the ASBL and $E_0 = 1.2 \times 10^{-7}$ for the BBL. In the case of the BBL, being the flow non-parallel, we do not impose periodicity in the streamwise direction. Thus, we have used a domain two times longer in x than that

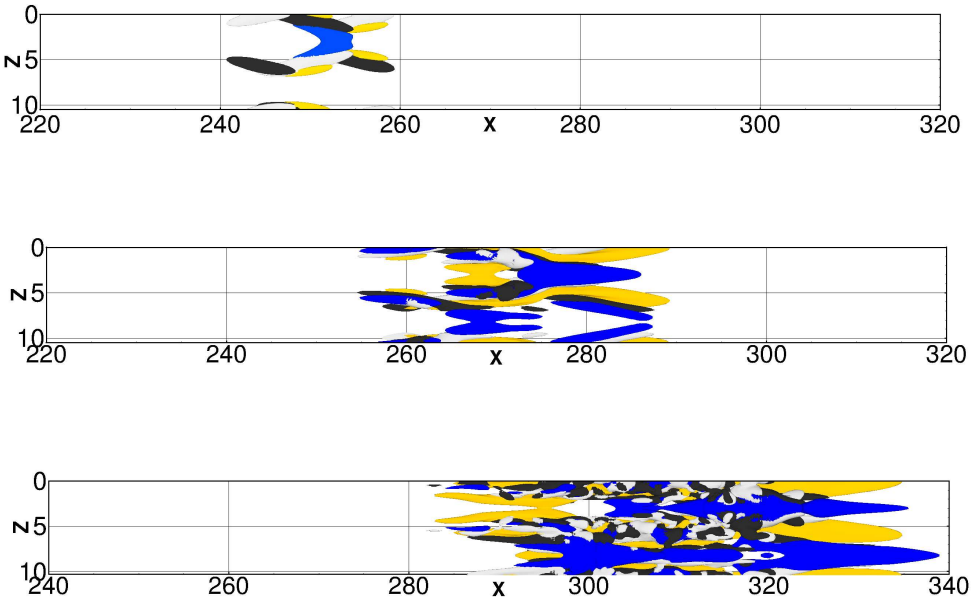

Figure 14: (Color online) Snapshots of the evolution in time of the selected NLOP for the BBL: iso-surfaces of the streamwise velocity and vorticity perturbations (yellow and blue, for $u' = \pm 0.1$, respectively; black and white, $\omega'_x = \pm 0.2$, respectively) at $t = 40, 80, 140$ (from top to bottom).

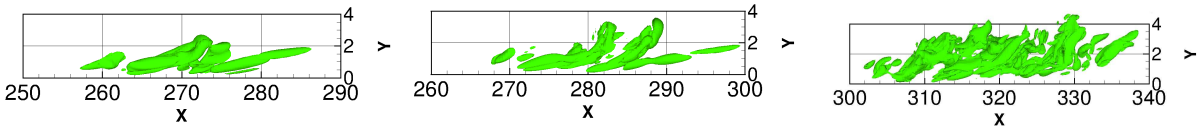

Figure 15: (Color online) Snapshots of the evolution in time of the selected NLOP for the BBL: isosurfaces of the Q-criterion for $t = 80, 100, 160$ (from left to right) .

used for the ASBL, in order to follow the evolution of the perturbation for a sufficiently long time before the disturbance leaves the domain. The number of grid points in the streamwise direction has been doubled as well, in order to maintain the same local grid resolution.

A qualitative picture of the transition process initiated by the NLOP for the ASBL is given in figure 13, showing the streamwise vorticity (black and white surfaces) and velocity (blue and yellow) perturbations. At $t = 40$ (first frame), the initial vortices increase their strength and streamwise inclination, due to the Orr mechanism [54]. This first phase is

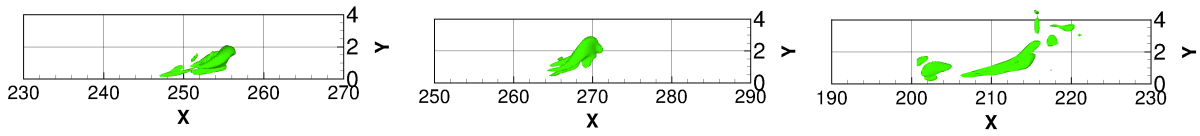

Figure 16: (Color online) Snapshots of the evolution in time of the selected NLOP for the ASBL: isosurfaces of the Q-criterion for $t = 80, 100, 160$ (from left to right) .

similar to that obtained for the BBL, and appears to depend on the action of the non-linear coupling terms linked to the components of the streamwise vorticity, such as ww_z, as explained in detail in Ref. [45]. At the same time, the streamwise velocity perturbation increases its amplitude, due to a *modified lift-up* effect [45]. In fact, since the initial vortices are inclined, the generated streaks are modulated in the streamwise direction, as shown in the second frame for $t = 80$. In particular, a main high-speed bent streak (yellow) is created, flanked by two weaker low-speed streaks. On such streaks, localized patches of vorticity are observed (see the third frame for $t = 140$), which are originated from the splitting of the initial inclined vortices. The bent streaks continue to be fed by the streamwise vortices, elongating in the streamwise direction, as shown in the fourth frame for $t = 200$. However, in the regions of larger vorticity, stronger modulations of the streaks are induced, leading the wave packet to break-up starting from a localized region. Such a scenario recalls the mechanism of secondary instability of streamwise streaks which triggers bypass transition in boundary-layer flows [11, 56]. In particular, since the initial disturbance is not mirror-symmetric, the streaks are characterized by sinuous oscillations, which represent the primary instabilities of streamwise streaks [10, 11]. However, in the non-linear optimal case, this mechanism is much more rapid than the one relying on the linear growth of streamwise-aligned streaks followed by saturation and secondary instability. In fact, the initial inclined vortices can create bent streaks in a short time and lead to break-up by-passing the secondary instability due to their spanwise modulations [57]. The non-linear transition process is similar to the first phases of the disturbance evolution on the periodic orbit recently found by bisection in a small domain (see Ref. [36]). However, since the NLOP considered here does not lay on the edge of chaos as the mentioned periodic orbit, transition to turbulence is reached after the bursting phase.

Despite the similarity of the initial optimal disturbances, the non-linear route to transition described here shows important differences with respect to that found in the non-parallel case. In fact, for the BBL case, the perturbation maintains the initial symmetry of the NLOP up to large times (obviously, before turbulence is initiated). As shown in figure 14, the initial mirror-symmetric inclined vortices transport the flow momentum causing an amplification of the streamwise component of velocity along them and inducing the creation of low- and high-momentum zones showing a Λ and an X shape, respectively (see the blue and yellow surfaces in the first frame for $t = 40$). This Λ structure of the perturbation is maintained at larger time (see the second frame for $t = 80$), and the mirror-symmetric inclined vortices connect their fronts to create a $\Lambda-$vortex, which eventually turns into a hairpin vortex leading the flow to break-up (third frame for $t = 140$). The formation of the hairpin for the BBL can be clearly seen in figure 15 at times $t = 80$ (a), $t = 100$, (b), and $t = 160$, where the green surfaces show the Q-criterion, highlighting the regions of high vorticity. At $t = 80$, one can observe that the initial vortices, tilted by the mean flow, are inclined at a small angle with respect to the streamwise axis ($\approx 7°$). However, at larger times, the vortices in the heart of the wave packet increase their inclination, reaching angles of about 35°. This phase coincides with the formation of the hairpin vortex (two of them are visible in the second frame at $t = 100$) which grows in size and splits into smaller hairpin vortices, leading very quickly to a turbulent spot (see the third frame at $t = 160$). On the other hand, for the ASBL, although the initial vortices have a similar wall-normal inclination with respect to the streamwise direction, as shown in the first and second frame of figure 16, the head of the hairpin vortex cannot be created due to the lack of symmetry of the perturbation. Thus, the vorticity does not spread in space as in the BBL case, but remains localized in a narrow region in the streamwise direction (see the third frame at $t = 160$).

The differences between the transition paths in the ASBL and BBL case can be analyzed by extracting the rms values of the three components of the velocity perturbation, as shown in figure 17, the thick lines referring to the ASBL, the thin ones to the BBL. In the BBL flow, the three components of velocity grow more rapidly and achieve larger rms values than in the ASBL case (see figure 17 (a)). Concerning the vorticity perturbation, shown in figure 17 (b), in the BBL case all of the three components grow more rapidly; the largest differences between the two flows are recovered for the wall-normal and spanwise vorticity, which attains values almost one order of magnitude larger than in the ASBL case. This can

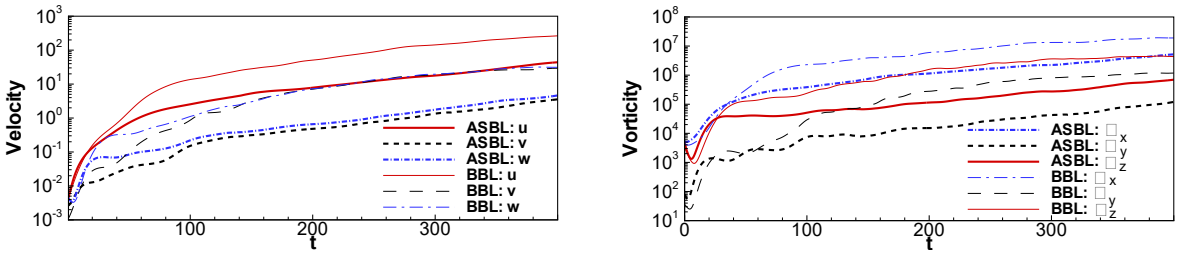

(a) (b)

Figure 17: (Color online) Evolution in time of the rms values of the three components of velocity (solid lines for u', dashed for v', dashed-dotted for w') (a) and vorticity (solid lines for ω'_z, dashed for ω'_y, dashed-dotted for ω'_x) (b) for a DNS initialized by the selected NLOP for the ASBL (thick lines) and the BBL (thin lines).

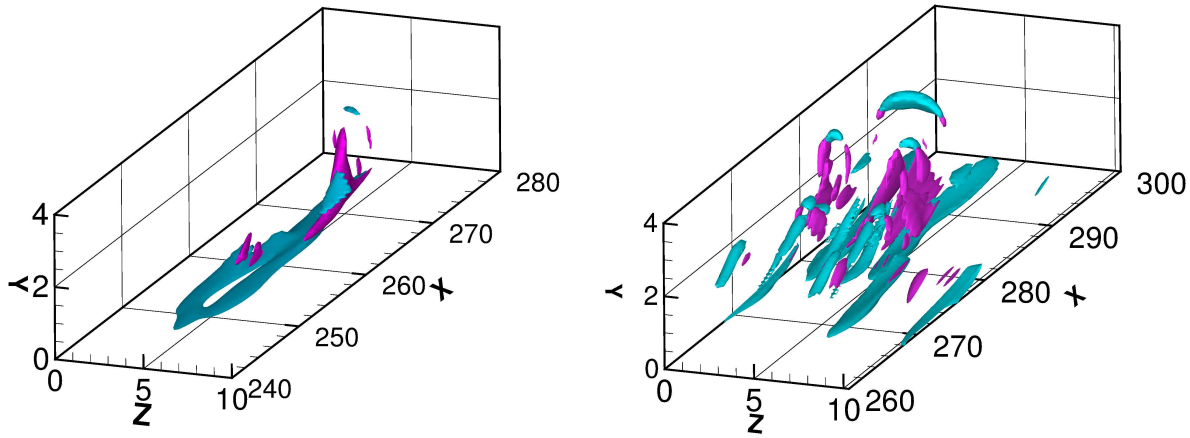

Figure 18: (Color online) Snapshots of the evolution in time of the selected NLOP for the ASBL (left frame) and the BBL (right frame): spanwise and wall-normal vorticity (blue surfaces for $\omega'_z = 0.8$, red ones for $\omega'_y = 0.65$.

be explained by observing that the vorticity components ω'_z and ω'_y have large values at the head and legs of the hairpin which characterize the BBL route to transition. In fact, plotting the ω'_z and ω'_y iso-surfaces for the parallel and non-parallel flow cases at $t = 100$, as provided in figure 18 (a) and (b), respectively, one can observe that these two components of the vorticity perturbations are much more extended in space and larger in magnitude in the non-parallel case than in the parallel one (both components are about 30%). In particular, the vorticity iso-surfaces are localized at the head and legs of the hairpin vortices, explaining

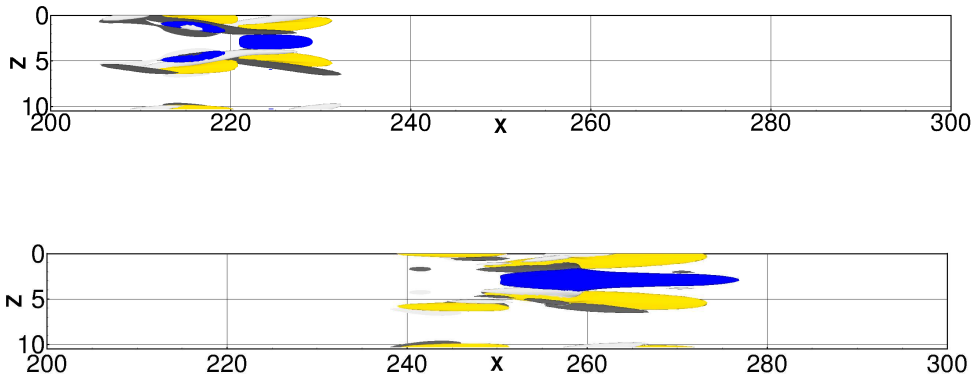

Figure 19: (Color online) Snapshots of the evolution in time of the selected NLOP obtained for the BBL, injected in the ASBL flow: iso-surfaces of the streamwise velocity and vorticity perturbations (yellow and blue, for $u' = \pm 0.1$, respectively; black and white, $\omega'_x = \pm 0.2$, respectively) at $t = 80, 140$ (from top to bottom).

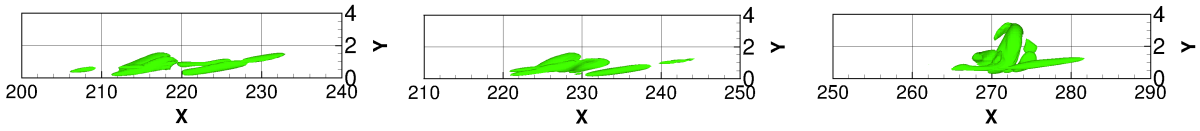

Figure 20: (Color online) Snapshots of the evolution in time of the selected NLOP obtained for the BBL, injected in the ASBL flow: isosurfaces of the Q-criterion for $t = 80, 100, 160$ (from left to right).

the larger growth of such terms with respect to the streamwise vorticity.

In order to better understand the differences between the two optimal transition paths, it is worth to analyze the evolution of the mirror-symmetric optimal perturbation superposed to the ASBL base flow at low Reynolds number. Thus, we inject the selected NLOP obtained for the BBL in the ASBL flow, and analyze its evolution in time. Figure 19 shows the streamwise vorticity (black and white) and velocity (yellow and blue) perturbations at $t = 80$ and $t = 140$. Comparing with figures 14 (b) and (c), one can observe that the vortices as well as the low- and high-momentum regions are straighten up and lose part of their inclination. As a result, at $t = 140$, three alternated streaks with weak vortices on their flanks are found. In particular, even if the initial perturbation is mirror-symmetric with respect to a

$z = const$ plane, the hairpin vortex is not formed at $t = 100$. This is clearly shown in figure 20, providing the Q-criterion iso-surfaces. One can see that at $t = 80$ (a) and at $t = 100$ (b) the inclination of the vortices is weak and begins to grow only at $t = 160$, turning eventually in a hairpin structure at $t \approx 200$. This can be also inferred by analyzing in figure 21 the time evolution of the rms value of the three velocity and vorticity components, and comparing them with the BBL case. As provided by the thick lines in figure 21 (a), the initial growth of the velocity components of the NLOP injected into the ASBL is initially similar to the one characterizing the BBL. However, at $t \approx 40$, the spanwise velocity component begins to decrease, and the wall-normal and the streamwise ones strongly decrease their growth rate. Concerning the vorticity components, at approximately the same time they all begin to decrease, the ${\omega'}_z$ and the ${\omega'}_y$ with a larger rate than the ${\omega'}_x$. This decrease is due to the absence of the hairpin vortex at $t \approx 100$; in fact, it begins to grow only at $t \approx 200$, when the growth of all of the vorticity components is observed, due to streaks breakdown of a varicose type. Thus, we can say that the mechanism of rapid formation of the hairpin, which is responsible for the strong growth of all of the vorticity components in the BBL case, is delayed for the ASBL due to the wall suction, making a "sinuous" instability mechanism more effective in inducing a rapid transition. A similar scenario is obtained in the case of the Couette flow [47]. Thus, in the case of the ASBL a mirror-symmetric optimal perturbation is less effective in inducing transition than a non-symmetric one. As observed in figure 16, the delay of the formation of the hairpin vortex appears to be due to the lower wall-normal inclination of the vortices with respect to the streamwise axis. This can be linked to a simple mechanism of transport of the perturbation by the mean flow. In fact, injecting the same initial vortical structure in the ASBL and the BBL base flows, in the latter case the highest part of the vortex will experience a lower streamwise base velocity as it is advected downstream, so it will decelerate with respect to its lowest part. This will induce an increase of the inclination of the initial vortex in the wall-normal direction, leading to a connection of the fronts of the two vortices, finally creating an hairpin structure. This is clearly shown in figure 22, providing the base flow vectors at $Re = 610$ for the ASBL (left frame) and the BBL (right frame) and the effect they have on the same vortical structure evolving in time up to $t = 100$. For the ASBL flow, the profile is fuller than the BBL one, so the mechanism of inclination by the mean flow is weaker, delaying the formation of the hairpin vortex from an initial mirror-symmetric perturbation. Therefore, the zones of strong velocity deficit (in

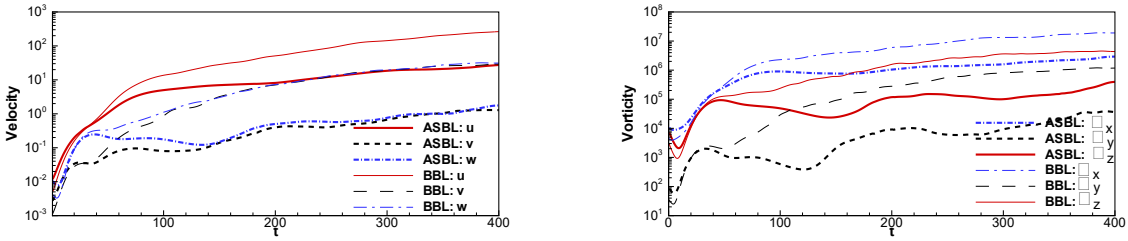

(a) (b)

Figure 21: (Color online) Evolution in time of the rms values of the three components of velocity (solid lines for u', dashed for v', dashed-dotted for w') (a) and vorticity (solid lines for ω'_z, dashed for ω'_y, dashed-dotted for ω'_x) (b) for a DNS initialized by the selected NLOP obtained for the BBL, injected into the ASBL (thick lines) and the BBL (thin lines) flows. .

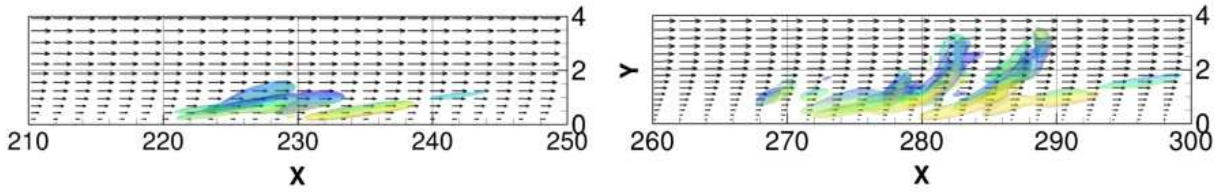

Figure 22: (Color online) Snapshots of the evolution in time of the selected NLOP obtained for the BBL at $Re = 610$, injected in the ASBL (left frame) and the BBL flow (right frame): isosurfaces of the Q-criterion for $t = 100$ and vectors of the base flow.

blue in the figure) remain closer to the wall, delaying the formation of inflection points in the mean flow profile, and the consequent transition to turbulence.

This conjecture can be verified by visualizing the activation of the transport terms of the spanwise vorticity (characterizing the head of the hairpin) by the mean flow. Figure 23 shows one of these two transport terms, Uv'_x, for the BBL (top frames) and the ASBL (bottom frames) at $t = 100$ (left frames) and $t = 150$ (right frames). It appears that, for the BBL, the terms is activated at the head of the hairpin vortices, spreading in space at larger time. Whereas, for the ASBL, it is characterized by a lower amplitude (lower than half the one for the BBL) and is rapidly damped in time. This confirms that the transport of the spanwise vorticity by the mean flow is indeed the mechanism which can explain the large differences in the symmetry of the two non-linear optimal perturbations. Such a result shows

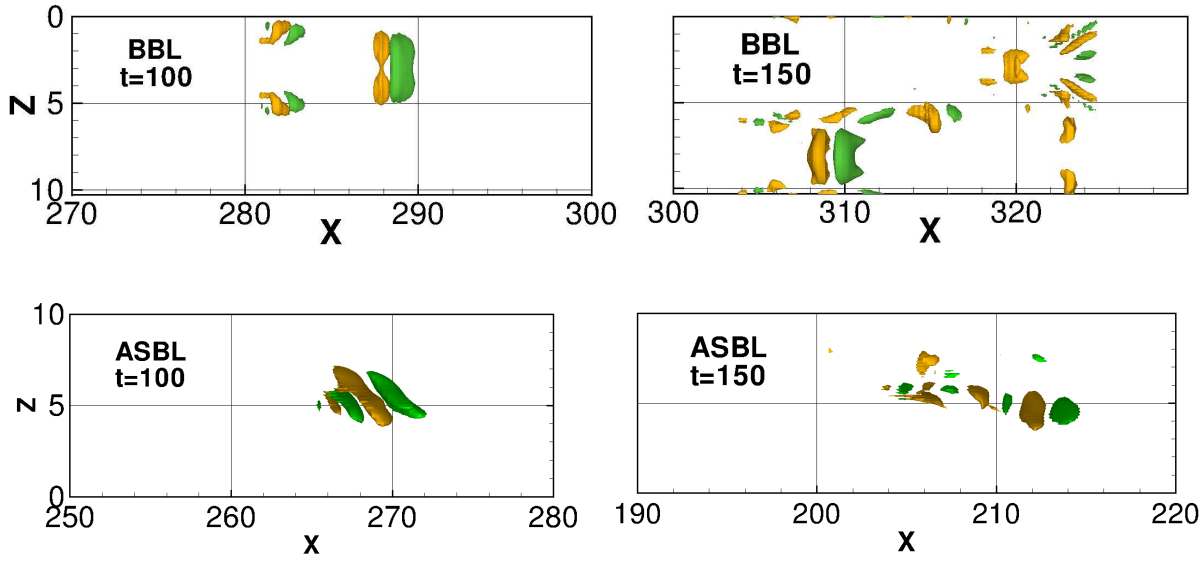

Figure 23: (Color online) Snapshots of the evolution in time of the advection term Uv'_x obtained for the BBL (top frames) and the ASBL (bottom frames) at $t = 100$ (left frames) and $t = 150$ (right frames): isosurfaces $Uv'_x = \pm 0.13$ for the BBL, $Uv'_x = \pm 0.06$ for the ASBL.

that it is crucial to take into account the non-linearity as well as the non-parallelism of a flow at the same time, for determining with accuracy the most effective route to transition. For larger Reynolds numbers, since the suction velocity V_S^* is much weaker, the mechanisms of tilting and stretching of the vortices tend to be closer to those of the BBL flow. Thus, the transition scenario tends to become similar to the BBL one, selecting mirror-symmetric perturbations as the optimal ones. Figure 24 shows three snapshots of the evolution in time of the NLOP obtained for $Re = 5000$ and $E_0 = 4.25 \times 10^{-9}$, showing a behaviour very similar to the one recovered for the BBL in figure 14. In particular, one can observe the formation of Λ structures for the negative streamwise velocity component and the streamwise vorticity. Figure 25 shows the generation of a train of hairpin vortices at $t = 75$ and $t = 100$, as well as the base flow profiles, which appear much less full than in the previous case. This confirms that wall suction is a crucial parameter for the stability of a boundary-layer flow, since, when it is strong enough, it can modify the dynamics of optimal perturbations and delay the formation of strongly growing vortical structures such as the hairpin vortices.

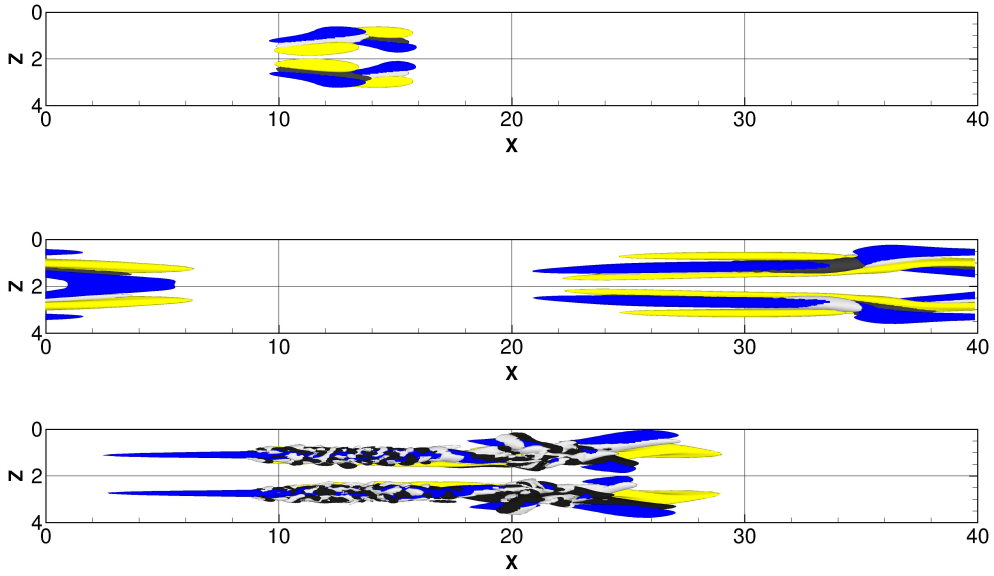

Figure 24: (Color online) Snapshots of the evolution in time of the symmetrical NLOP at $Re = 5000$, with initial energy $E_0 = 4.25 \times 10^{-9}$, extracted at $t = 50, 100, 150$, from top to bottom. The isosurfaces represent the streamwise velocity and vorticity perturbations (yellow and blue, for $u' = \pm 0.015, 0.03, 0.1$, from top to bottom; black and white, $\omega'_x = \pm 0.15, 0.1, 0.25$, from top to bottom).

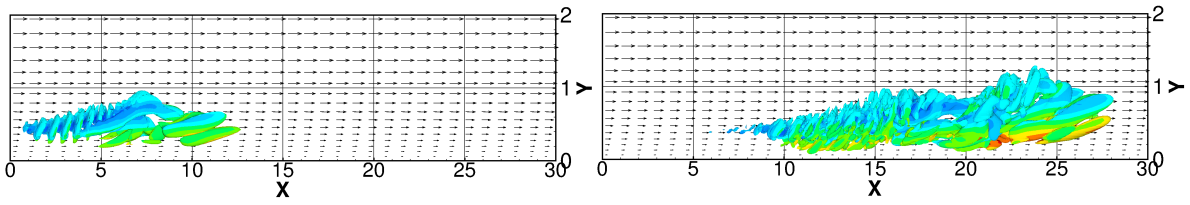

Figure 25: (Color online) Snapshots of the evolution in time of the selected NLOP obtained for the ASBL at $Re = 5000$, extracted at $t = 75$ (left frame) and $t = 100$ (right frame): isosurfaces of the Q-criterion ($Q = 20$) and vectors of the base flow.

IV. SUMMARY

A variational procedure has been employed to find *non-linear* optimal disturbances in the asymptotic suction boundary-layer (ASBL) flow. These perturbations are defined as

the ones yielding the largest energy growth at a given target time T, for a given Reynolds number Re. The results have been compared with those obtained using the same approach in the case of the Blasius boundary layer (BBL) flow [44]. The influence of the different structure of the ASBL velocity profile with respect to the BBL on the non-linear optimal growth mechanism has been studied. It has been found that suction remarkably reduces the optimal energy gain in the non-linear case. Moreover, the optimal perturbation obtained in the present case shares the same basic structure found for different shear flows such as the BBL and the Couette flows. However, unlike the BBL case, the optimal perturbation for the ASBL flow in the range of low to moderate Reynolds numbers, is not spanwise-symmetric. In particular, it has been found that a value of the Reynolds number exists between 5000 and 10000 for which the non-linear optimal perturbation changes from a non symmetric shape to a symmetric one. Therefore, for sufficiently high Reynolds numbers (low suction velocity for a given freestream velocity), the structure of the non-linear optimal disturbance becomes similar to the one of the BBL. By bisecting the initial energy of the non-linear optimal perturbations, minimal energy thresholds for subcritical transition to turbulence have been obtained. These energy thresholds are found to be 1 to 4 order of magnitude lower than the ones found in other transition scenarios such as secondary instability of elongated streamwise vortices, random noise, oblique waves and localized streamwise-aligned disturbances [23]. For $610 < Re < 5000$, these thresholds are found to scale with Re^{-2}, suggesting a new scaling law for transition in the ASBL.

Finally, direct numerical simulations show that the different structure of the base flow with respect to the BBL leads to a different evolution of the initial perturbation. In fact, unlike the case of the BBL flow, for low to moderate values of the Reynolds number, the formation of hairpin vortices is not observed in the transition process before break-up to turbulence, and a sinuous transition scenario is observed. This appears to be due to the lower tilting of the vortices induced by the fuller velocity profile in the ASBL case, which delay the formation of those vortical structures, which are able to rapidly lead the flow to transition. However, when wall suction is not strong enough (i.e., at large Re, for a given freestream velocity) the vorticity transport and tilting mechanism responsible for the formation of the hairpin vortex, is observed again. Future work will aim at investigate the existence of a similar change of symmetry in the non-linear optimal perturbations for different shear flows such as the plane Poiseuille flow, as well as the influence of the independent parameters of

the optimisation, such as the initial energy and the target time, on the optimal perturbation structure.

Acknowledgments

Some computations have been performed on the Power 6 of the IDRIS, France.

---

[1] H. Schlichting, "Boundary layer theory ," *Springer*, 2004.

[2] J. D. J. Anderson, "Ludwig prandtl's boundary layer," *Physics Today*, vol. 58, pp. 42–48, 2005.

[3] A. A. Griffith and F. W. Meredith, "The possible improvement in aircraft performance due to boundary layer suction," *Rep. Aero. Res. Coun.*, vol. Tech. Rep. N. E3501, 1936.

[4] L. M. Hocking, "Non-linear instability of the asymptotic suction velocity profile ," *Q. J. Mech. Appl. Maths*, vol. 28, pp. 341–353, 1975.

[5] R. D. Joslin, "Aircraft Laminar Flow Control ," *AIAA Paper*, vol. 97, p. 0625, 1998.

[6] M. Matsubara and P. Alfredsson, "Disturbance growth in boundary layers subjected to free-stream turbulence ," *J. Fluid Mech.*, vol. 430, pp. 149–168, 2001.

[7] J. Fransson, M. Matsubara, and P. H. Alfredsson, "Transition induced by free stream turbulence ," *J. Fluid Mech.*, vol. 527, no. 10, pp. 1–25, 2005.

[8] P. S. Klebanoff, "Effects of freestream turbulence on the laminar boundary layer ," *Bull Am. Phys. Soc.*, vol. 10, no. 1323, 1971.

[9] M. T. Landahl, "A note on an algebraic instability of inviscid parallel shear flows ," *J. Fluid Mech.*, vol. 98, pp. 243–251, 1980.

[10] P. Andersson, L. Brandt, A. Bottaro, and D. S. Henningson, "On the breakdown of boundary layer streaks ," *J. Fluid Mech.*, vol. 428, pp. 29–60, 2001.

[11] L. Brandt, P. Schlatter, and D. S. Henningson, "Transition in a boundary layers subject to free-stream turbulence ," *J. Fluid Mech.*, vol. 517, pp. 167–198, 2004.

[12] J. Hoepffner, L. Brandt, and D. S. Henningson, "Transient growth on boundary layer streaks ," *J. Fluid Mech.*, vol. 537, pp. 91–100, 2005.

[13] K. M. Butler and B. F. Farrell, "Three-dimensional optimal perturbations in viscous shear flow ," *Phys. Fluids A*, vol. 4, pp. 1637–1650, 1992.

[14] S. C. Reddy and D. S. Henningson, "Energy growth in viscous channel flows ," *J. Fluid Mech.*, vol. 252, pp. 209–238, 1993.

[15] P. Corbett and A. Bottaro, "Optimal perturbations for boundary layers subject to stream-wise pressure gradient ," *Phys. Fluids*, vol. 12, pp. 120–130, 2000.

[16] P. Andersson, M. Berggren, and H. D. S., "Optimal disturbances and byoass transition in boundary layers ," *Phys. Fluids*, vol. 11, no. 1, pp. 134–150, 1999.

[17] P. Luchini, "Reynolds number indipendent instability of the Blasius boundary layer over a flat surface: optimal perturbations ," *J. Fluid Mech.*, vol. 404, pp. 289–309, 2000.

[18] B. Farrell, "Optimal excitation of perturbations in viscous shear flow ," *Phys. Fluids*, vol. 31, pp. 2093–2102, 1988.

[19] P. Luchini and Bottaro, "Adjoint Equations in Stability Analysis ," *Ann. Rev. Fluid Mech.*, vol. 46, pp. 493–517, 2014.

[20] J. H. M. Fransson and P. H. Alfredsson, "On the disturbance growth in an asymptotic suction boundary layers ," *J. Fluid Mech.*, vol. 482, pp. 51–90, 2003.

[21] J. H. M. Fransson and P. Corbett, "Optimal linear growth in the asymptotic suction boundary layer ," *Eur. J. Mech./Fluids*, vol. 22, pp. 259–270, 2003.

[22] M. Bystrom, O. Levin, and D. S. Henningson, "Optimal disturbances in suction boundary layers ," *Eur. J. Mech. B/Fluids*, vol. 26, pp. 330–343, 2007.

[23] O. Levin, N. Davidsson, and D. S. Henningson, "Transition thresholds in the asymptotic suction boundary layer ," *Physics of Fluids. A, Fluid Dynamics*, vol. 17, p. 114104, 2005.

[24] O. Levin and D. S. Henningson, "Turbulent spots in the asymptotic suction boundary layer ," *J. Fluid Mech*, vol. 548, pp. 397–413, 2007.

[25] M. Nagata, "Three-dimensional finite amplitude solutions in plane Couette flow ," *J. Fluid Mech.*, vol. 217, pp. 519–527, 1990.

[26] F. Waleffe, "Three-dimensional states in plane shear flow ," *Phys. Rev. Lett.*, vol. 81, pp. 4140–4143, 1998.

[27] B. Hof, C. van Doorne, J. Westerweel, F. Nieuwstadt, H. Faisst, B. Eckhardt, H. Wedin, R. Kerswell, and F. Waleffe, "Experimental Observation of Nonlinear Traveling Waves in Turbulent Pipe Flow ," *Science*, vol. 305, pp. 1594–1598, 2004.

[28] H. Wedin and R. Kerswell, "Exact coherent structures in pipe flow: travelling wave solutions ," *J. Fluid Mech.*, vol. 508, pp. 333–371, 2004.

[29] B. Eckhardt, T. M. Schneider, B. Hof, and J. Westerweel, "Turbulence transition of pipe flow ," *Annu. Rev. Fluid Mech.*, vol. 39, pp. 447–468, 2007.

[30] D. Viswanath and P. Cvitanovic, "Stable manifolds and the transition to turbulence in pipe flow ," *J. Fluid Mech.*, vol. 627, p. 215, 2009.

[31] J. D. Skufca, J. Yorke, and B. Eckhardt, " Edge of chaos in a parallel shear flow ," *Phys. Rev. Lett.*, vol. 96, p. 174101, 2006.

[32] T. M. Schneider, B. Eckhardt, and J. Yorke, " Turbulence Transition and the Edge of Chaos in Pipe Flow ," *Phys. Rev. Lett.*, vol. 99, p. 034502, 2007.

[33] S. Cherubini, P. De Palma, J.-C. Robinet, and A. Bottaro, "Edge states in a boundary layer ," *Phys. of Fluids*, vol. 23, p. 051705, 2011.

[34] Y. Duguet, A. Monokrousos, L. Brandt, and D. S. Henningson, "Minimal transition thresholds in plane Couette flow ," *Phys. Fluids*, vol. 25, p. 084103, 2013.

[35] T. M. Schneider, J. F. Gibson, M. Lagha, F. De Lillo, and B. Eckhardt, "Laminar-turbulent boundary in plane Couette flow ," *Phys. Rev. E*, vol. 78, p. 037301, 2008.

[36] T. Kreilos, G. Veble, T. M. Schneider, and B. Eckhardt, "Edge states for the turbulence transition in the asymptotic suction boundary layer ," *J. Fluid Mech.*, vol. 726, pp. 100–122, 2013.

[37] T. Khapko, T. Kreilos, P. Schlatter, Y. Duguet, B. Eckhardt, and D. Henningson, "Localized edge states in the asymptotic suction boundary layer ," *J. Fluid Mech.*, vol. 717, p. R6, 2013.

[38] T. Khapko, Y. Duguet, T. Kreilos, P. Schlatter, B. Eckhardt, and D. Henningson, "Complexity of localised coherent structures in a boundary-layer flow ," *The European Physical Journal E*, vol. 37, pp. 1–12, 2014.

[39] S. Rabin, C. P. Caulfield, and R. Kerswell, "Triggering turbulence efficiently in plane Couette flow ," *J. Fluid Mech.*, vol. 712, pp. 244–272, 2012.

[40] S. Cherubini and P. De Palma, "Minimal perturbations approaching the edge of chaos in a Couette flow ," *Fluid Dynamics Research*, vol. 46, p. 041403, 2014.

[41] R. R. Kerswell, C. C. T. Pringle, and A. P. Willis, "An optimisation approach for analysing nonlinear stability with transition to turbulence in fluids as an exemplar ," *Rep. Prog. Phys.*, vol. 77, p. 085901, 2014.

[42] C. C. T. Pringle and R. Kerswell, "Using nonlinear transient growth to construct the minimal seed for shear flow turbulence ," *Phys. Rev. Lett.*, vol. 105, p. 154502, 2010.

[43] C. C. T. Pringle, A. Willis, and R. Kerswell, "Minimal seeds for shear flow turbulence: using nonlinear transient growth to touch the edge of chaos ," *J. Fluid Mech.*, vol. 702, pp. 415–443, 2011.

[44] S. Cherubini, P. De Palma, J.-C. Robinet, and A. Bottaro, "Rapid path to transition via nonlinear localized optimal perturbations ," *Phys. Rev. E*, vol. 82, p. 066302, 2010.

[45] S. Cherubini, P. De Palma, J.-C. Robinet, and A. Bottaro, "The minimal seed of turbulence transition in a boundary layer ," *J. Fluid Mech.*, vol. 689, pp. 221–253, 2011.

[46] A. Monokrousos, A. Bottaro, L. Brandt, A. Di Vita, and D. S. Henningson, " Non-equilibrium thermodynamics and the optimal path to turbulence in shear flows ," *Phys. Rev. Lett.*, vol. 106, p. 134502, 2011.

[47] S. Cherubini and D. Palma, "Nonlinear optimal perturbations in a Couette flow: bursting and transition ," *J. Fluid Mech.*, vol. 716, pp. 251–279, 2012.

[48] S. Cherubini, P. De Palma, J.-C. Robinet, and A. Bottaro, "A purely nonlinear route to transition approaching the edge of chaos in a boundary layer ," *Fluid Dynamics Research*, vol. 44, p. 031404, 2012.

[49] S. Cherubini, J.-C. Robinet, and P. De Palma, "Nonlinear control of unsteady finite-amplitude perturbations in the Blasius boundary-layer flow ," *J. Fluid Mech.*, vol. 737, pp. 440–465, 2013.

[50] S. Rabin, C. P. Caulfield, and R. Kerswell, "Designing a more nonlinearly stable laminar flow via boundary manipulation," *J. Fluid Mech.*, vol. 738, p. R1, 2014.

[51] R. Verzicco and P. Orlandi, " A finite-difference scheme for the three-dimensional incompressible flows in cylindrical coordinates ," *J. Comp. Phys.*, vol. 123, no. 2, pp. 402–414, 1996.

[52] S. Zuccher, P. Luchini, and A. Bottaro, "Algebraic growth in a blasius boundary layer: optimal and robust control by mean suction in the nonlinear regime," *Eur. J. Mech. B/Fluids*, vol. 513, pp. 135–160, 2004.

[53] S. Cherubini, J.-C. Robinet, A. Bottaro, and P. De Palma, "Optimal wave packets in a boundary layer and initial phases of a turbulent spot ," *J. Fluid Mech.*, vol. 656, pp. 231–259, 2010.

[54] W. M. F. Orr, "The stability or instability of the steady motions of a liquid. Part I ," *Proceedings of the Royal Irish Academy, A*, vol. 27, pp. 9–68, 1907.

[55] S. Yoshioka, J. H. M. Fransson, and P. H. Alfredsson, "Free stream turbulence induced disturbances in boundary layers with wall suction ," *Phys. Fluids*, vol. 16, p. 3530, 2004.

[56] W. Schoppa and F. Hussain, "Coherent structure generation in near-wall turbulence ," *J. Fluid*

Mech., vol. 453, pp. 57–108, 2002.

[57] F. Waleffe, "On a self-sustaining process in shear flows ," *Phys. Fluids*, vol. 9, pp. 883–901, 1997.